

Universal Dynamics with Globally Controlled Analog Quantum Simulators

Hong-Ye Hu,^{1,*} Abigail McClain Gomez,^{1,†} Liyuan Chen,^{1,2,†} Aaron Trowbridge,^{3,4} Andy J. Goldschmidt,⁵ Zachary Manchester,³ Frederic T. Chong,⁵ Arthur Jaffe,^{1,6} and Susanne F. Yelin^{1,‡}

¹*Department of Physics, Harvard University, Cambridge, MA 02138, USA*

²*School of Engineering and Applied Sciences, Harvard University, Allston, MA 02134, USA*

³*Robotics Institute, Carnegie Mellon University, Pittsburgh, PA 15213, USA*

⁴*HarmoniQs, Inc.*

⁵*Department of Computer Science, University of Chicago, Chicago, IL 60637, USA*

⁶*Department of Mathematics, Harvard University, Cambridge, Massachusetts 02138, USA*

(Dated: August 27, 2025)

Analog quantum simulators with global control fields have emerged as powerful platforms for exploring complex quantum phenomena. Recent breakthroughs, such as the coherent control of thousands of atoms, highlight the growing potential for quantum applications at scale. Despite these advances, a fundamental theoretical question remains unresolved: to what extent can such systems realize universal quantum dynamics under global control? Here we establish a necessary and sufficient condition for universal quantum computation using only global pulse control, proving that a broad class of analog quantum simulators is, in fact, universal. We further extend this framework to fermionic and bosonic systems, including modern platforms such as ultracold atoms in optical superlattices. Crucially, to connect the theoretical possibility with experimental reality, we introduce a new control technique into the experiment — *direct quantum optimal control*. This method enables the synthesis of complex effective Hamiltonians and allows us to incorporate realistic hardware constraints. To show its practical power, we experimentally engineer three-body interactions outside the blockade regime and demonstrate topological dynamics on a Rydberg atom array. Using the new control framework, we overcome key experimental challenges, including hardware limitations and atom position fluctuations in the non-blockade regime, by identifying smooth, short-duration pulses that achieve high-fidelity dynamics. Experimental measurements reveal dynamical signatures of symmetry-protected-topological edge modes, confirming both the expressivity and feasibility of our approach. Our work opens a new avenue for quantum simulation beyond native hardware Hamiltonians, enabling the engineering of effective multi-body interactions and advancing the frontier of quantum information processing with globally-controlled analog platforms.

I. INTRODUCTION

Precise analog pulse control lies at the foundation of all modern quantum technology. Building on this physical principle, two main paradigms of programmable quantum platforms have emerged: digital quantum computers and analog quantum simulators. In recent years, digital quantum computers have often drawn the spotlight. Remarkable progress in these devices has enabled fault-tolerant quantum error correction that surpasses the break-even point of noise [1–5]. At the hardware level, digital quantum computers rely on continuous-time analog dynamics governed by carefully shaped control pulses, which implement the local, few-qubit gates necessary for computation [6–8]. In parallel, there has been rapid progress in the development of analog quantum simulators with global control fields. Recent experiments have demonstrated coherent manipulation of hundreds to thousands of atoms and ions [9–15]. These globally-controlled analog platforms have emerged as leading candidates for scaling to large system sizes compared to digital architectures that require fully local control.

Although there have been many compelling demonstrations of analog quantum simulation in the study of quantum many-body physics, such as the exploration of complex out-of-equilibrium phenomena [16–21], superconductivity [22–27], topological phases [28–31], and lattice gauge theories [32, 33], analog simulators are still often perceived as being limited to emulating Hamiltonians closely tied to their native physical interactions. To bridge the gap between analog and digital quantum platforms, a fundamental theoretical question must be addressed: to what extent can analog systems realize universal quantum dynamics under global control?

In this work, we address this question with a surprisingly simple necessary and sufficient condition for achieving universal quantum computation using only global pulse control. Our approach relies on the tool of dynamical Lie algebras [34]. In contrast to previous studies [35–38], which analyze specific systems on a case-by-case basis, our

* These authors contributed equally to this work.; Corresponding author: hongyehu@fas.harvard.edu

† These authors contributed equally to this work.

‡ Corresponding author: syelin@g.harvard.edu

condition is independent of the detailed structure of the physical Hamiltonians. A striking implication is that a broad class of analog quantum simulators are, in fact, capable of universal quantum computation when equipped with appropriate global control pulses. We further extend this framework to establish universal simulation in fermionic and bosonic systems, including modern platforms such as ultracold atoms in optical superlattices [39–41].

$$\begin{array}{ccc} \text{Dynamical Lie Algebra + Direct Quantum Optimal Control} & \implies & \text{Useful Universal Analog Simulator} \\ \text{(Theory)} & & \text{(Experiment)} \end{array}$$

While the theory of dynamical Lie algebras tells us what is achievable with global pulse engineering, it is not constructive. As suggested by the main thematic equation above, realizing a useful and universal analog quantum simulator also requires a practical tool. To this end, we introduce a new quantum control technique into the experimental workflow: direct quantum optimal control. Originally developed in the context of aerospace and robotics [42–44], this method treats both the analog control pulses and the quantum states (or unitaries) at each time point as trainable parameters, with the Schrödinger equation imposed as a constraint. In contrast to conventional pulse control methods such as Floquet engineering [45–49] and Gradient Ascent Pulse Engineering (GRAPE) [50] (categorized as indirect methods), direct quantum optimal control allows the optimization algorithm to initialize and explore “nonphysical” regions — these are points in the joint state and control trajectory space that are *infeasible*, i.e., they do not satisfy the dynamics constraints — during intermediate steps before convergence to a feasible solution. This greater flexibility in finding effective solutions makes direct methods particularly well suited for realistic experimental settings involving multiple hardware constraints, where traditional techniques often struggle with local minima or fail to accommodate system limitations.

In this work, we combine our new developments in both theory and experiment to demonstrate the potential of globally controlled analog quantum simulators. To substantiate the power of our approach, we focus on Rydberg atom arrays with van der Waals interactions. Qubits are encoded in the ground and Rydberg states, which are also known as the analog encoding. Although the native Hamiltonian contains only long-range two-body interactions, we demonstrate the engineering of effective *three-body* interactions using global pulse control. As a concrete example, we focus on the synthesis of a ZXZ Hamiltonian, which lies in a symmetry-protected topological (SPT) phase [51].

In Rydberg analog quantum simulation, previous experiments have typically operated within the Rydberg blockade regime, where strong native two-body interactions enable high-precision control [6, 52–55]. However, using the theoretical tools we developed, we show that the ZXZ Hamiltonian cannot be realized within the typical blockade regime but becomes possible outside it. To achieve this goal, we overcome several key experimental challenges. The first is decoherence arising from the residual atomic temperature, since atoms are untrapped during evolution in the analog encoding. We develop a phenomenological model that captures this process well. In addition to thermal motion, we must also satisfy strict constraints on the laser control parameters, further increasing the experimental complexity. Using our control framework, we identify smooth, short-duration pulses that achieve high-fidelity dynamics. Experimental measurements reveal dynamical signatures of symmetry-protected topological edge modes, confirming both the expressivity and experimental feasibility of our approach.

Our work paves a new path for analog quantum simulation through advanced pulse control techniques that go beyond the native Hamiltonians of the simulators. It significantly expands the expressive power of analog platforms and lays the foundation for simulating exotic quantum many-body phenomena through synthesized multi-body interactions, as well as for large-scale quantum information processing using analog quantum devices.

II. UNIVERSAL QUANTUM COMPUTATION UNDER GLOBAL CONTROLS

A. Minimal requirement for universal quantum computation

The Hilbert space of an N -qubit system is the N -fold tensor product of \mathbb{C}^2 , i.e., $\mathcal{H}_q = (\mathbb{C}^2)^{\otimes N}$. Given a set of time-dependent control pulses $\mathbf{u}(t)$, the dynamics of an analog system are governed by a time-dependent Hamiltonian of the form $H(t) = \sum_{\alpha} u_{\alpha}(t)H_{\alpha}$. Here, $H_{\alpha} \in \{H_1, H_2, \dots, H_l\}$ is a set of basic control Hamiltonians, and $u_{\alpha}(t)$ is the corresponding component of the control pulse vector $\mathbf{u}(t)$. More concretely, the unitary dynamics generated by $H(t)$ is given by:

$$U = \mathcal{T} \left[e^{-i \int H(t) dt} \right] = \mathcal{T} \left[e^{-i \int \sum_{\alpha} u_{\alpha}(t) H_{\alpha} dt} \right], \quad (1)$$

where \mathcal{T} denotes time-ordering. A system is said to be universal or to realize universal quantum computation (UQC) if we can approximate any target unitary V on \mathcal{H}_q by U . To be precise, given any target unitary $V \in \text{SU}(2^N)$ and

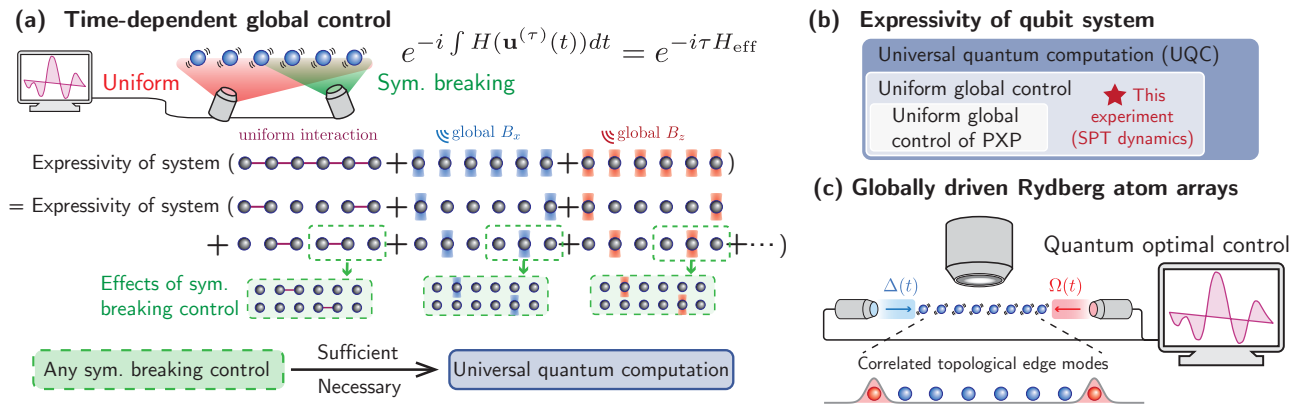


FIG. 1. **Expressivity of globally controlled analog quantum simulators.** (a) An analog quantum system is driven by uniform global control fields (red) and an additional symmetry-breaking field (green). The uniform controls allow for almost individual controllability of local fields and interactions, except for a remaining reflection symmetry that couples qubits at mirrored positions (e.g., the first and last qubits). We prove that adding any global field that breaks this symmetry is both necessary and sufficient for universal quantum computation. (b) Expressivity diagram of qubit systems. While uniform global control is not universal, it still enables access to exponentially many effective Hamiltonians. Our experiment (red star) realizes symmetry-protected topological (SPT) dynamics with three-body ZZ interactions using only uniform global control. (c) Experimental setup. A Rydberg atom array is globally controlled outside the blockade regime with time-dependent detuning $\Delta(t)$ and Rabi frequency $\Omega(t)$. Employing quantum optimal control, we engineer three-body interactions and observe dynamical signatures of topological edge modes.

any desired precision ϵ , there exists a control sequence $\mathbf{u}(t)$ such that $\|U - V\|_{\diamond} \leq \epsilon$, where $\|\cdot\|_{\diamond}$ is the diamond norm between quantum channels [56–58].

In this work, we investigate UQC in globally-controlled systems. We denote the support of a basic control Hamiltonian H_{α} , i.e., the qubits it acts nontrivially on, by $\text{Supp}(H_{\alpha})$. If all control fields have extensive support, namely $|\text{Supp}(H_{\alpha})| = \mathcal{O}(N)$ for all H_{α} , we say the system is globally-controlled. In such systems, only $\mathcal{O}(1)$ independent control fields are required, significantly simplifying experimental implementation. By contrast, traditional approaches to UQC rely on universal local gate sets, such as the Clifford plus T gates [59], where each gate acts on only a small constant number of qubits, i.e. $|\text{Supp}(H_{\alpha})| = \mathcal{O}(1)$ for each H_{α} . These local control schemes require full spatial addressability of individual qubits, with the number of controls scaling as $\mathcal{O}(N)$. This demand introduces considerable experimental overhead compared to global control. Therefore, it naturally raises the question: is an extensive amount of local control necessary for UQC, or can one achieve universality using only a small number of global control fields, independent of system size?

Surprisingly, the latter is possible. In a pioneering work, Benjamin [36] showed that a globally-controlled quantum dot system with alternating on-off interactions can realize universal computation. Recently, it has been shown that this question is also related to the expressivity of variational quantum algorithms, where the control pulses $\mathbf{u}(t)$ serve as trainable parameters [60–62]. In this context, Lloyd [37] demonstrated that a globally controlled variant of the Quantum Approximate Optimization Algorithm (QAOA) is universal. However, previous studies of universality under global control have primarily followed a case-by-case analysis for a specific set of control Hamiltonians $\{H_{\alpha}\}$. To approach the problem from a fundamental perspective, we move beyond such examples and establish a necessary and sufficient condition for UQC under global control.

To this end, we first identify the most natural framework for globally-controlled analog quantum simulators, within which we investigate the conditions required for universality. Without loss of generality, we consider a one-dimensional chain of qubits, and the generalization to higher-dimensional lattices is straightforward (see discussions in Appendix B). Notably, each two-level system functions as a qubit when it can undergo rotations about the X - and Z -axes, implemented via suitable control pulses. Furthermore, the physical nature of typical quantum platforms enables interactions between neighboring qubits. Therefore, in a globally-controlled architecture, the minimal set of controls consists of uniform X - and Z -rotations applied to all qubits, described by the Hamiltonians $H_X = \sum_i X_i$ and $H_Z = \sum_i Z_i$, and uniform nearest-neighbor interactions. Even though the exact form of the interaction is not essential (see Appendix B), for convenience, we consider it to be of the Ising type, given by $H_{ZZ} = \sum_{\langle i,j \rangle} Z_i Z_j$. The system is thus governed by the Hamiltonian

$$H_q(t) = u_X(t)H_X + u_Z(t)H_Z + u_{ZZ}(t)H_{ZZ} = u_X(t) \sum_i X_i + u_Z(t) \sum_i Z_i + u_{ZZ}(t) \sum_{\langle i,j \rangle} Z_i Z_j. \quad (2)$$

As a one-dimensional open chain, the system has only lattice reflection symmetry about its center. We identify this geometrical symmetry as the sole obstruction to universality. Specifically, by introducing *any* additional control term H_{break} that breaks this symmetry, the system becomes capable of UQC. This result is formalized in Theorem 1.

Theorem 1 (Minimal requirement for universal quantum computation on a qubit chain). *Consider a chain of qubits with homogeneous nearest-neighbor interactions. Suppose the system is equipped with tunable global X and Z fields, given by $H_X = \sum_j X_j$, $H_Z = \sum_j Z_j$. Then, this system realizes universal quantum computation if and only if there exists at least one additional control field that breaks the lattice reflection symmetry.*

To prove this result, we employ a tool known as the dynamical Lie algebra (DLA), originally developed in quantum control theory [34, 63] and recently also applied to variational quantum algorithms [60–62, 64]. Intuitively, given a set of control Hamiltonians $\{H_1, H_2, \dots, H_l\}$, one can construct the linear space $\mathcal{V} = \text{span}_{\mathbb{R}}\langle \cup_{j=1}^l iH_j \rangle_{\text{Lie}}$, defined as the span of all possible nested commutators, i.e., operators of the form $[[\dots [iH_i, iH_j], \dots], iH_k]$, over the real numbers. It can be shown that for any anti-Hermitian operator $L \in \mathcal{V}$, the corresponding unitary e^{-L} can be approximated to arbitrary precision ϵ by designing an appropriate control sequence $\mathbf{u}(t)$ (see Lemmas 2 and 3 in Appendix A). Therefore, a dynamical system governed by Equation (1) is said to be universal if $\text{span}_{\mathbb{R}}\langle \cup_{j=1}^l iH_j \rangle_{\text{Lie}} = \text{span}_{\mathbb{R}}\langle i\mathbb{P}_N \setminus \mathbb{I} \rangle_{\text{Lie}}$, where $\mathbb{P}_N \setminus \mathbb{I}$ denotes the set of all N -qubit Pauli operators \mathbb{P}_N excluding the identity operator \mathbb{I} . This tool enables us to study the expressivity of dynamical systems without considering the details of $\mathbf{u}(t)$ and instead focusing on the important control Hamiltonians H_α .

A well-known universal gate set is generated by single-qubit X - and Z -rotations plus arbitrary nearest-neighboring-qubit interactions [65]. Formally speaking, the generators X_j, Z_j and $Z_j Z_{j+1}$ for all site j span the whole $\mathfrak{su}(2^N)$ Lie algebra, i.e., $\text{span}_{\mathbb{R}}\langle \cup_j iX_j, \cup_j iZ_j, \cup_j iZ_j Z_{j+1} \rangle_{\text{Lie}} = \text{span}_{\mathbb{R}}\langle i\mathbb{P}_N \setminus \mathbb{I} \rangle_{\text{Lie}}$. Surprisingly, we found that the uniform controls, as in Equation (2), allow for almost individual controllability of local fields and interactions, except for a remaining reflection symmetry that couples qubits at mirrored positions (e.g., the first and last qubits). Given the reflection operation \mathcal{R} yielding $\mathcal{R}(X_j/Z_j) = X_{(N-j)+1}/Z_{(N-j)+1}$, the uniform control Hamiltonians generate the following DLA:

$$\text{span}_{\mathbb{R}}\langle iH_X, iH_Z, iH_{ZZ} \rangle_{\text{Lie}} = \text{span}_{\mathbb{R}}\langle \cup_j i(X_j + \mathcal{R}(X_j)), \cup_j i(Z_j + \mathcal{R}(Z_j)), \cup_j i(Z_j Z_{j+1} + \mathcal{R}(Z_j)\mathcal{R}(Z_{j+1})) \rangle_{\text{Lie}}, \quad (3)$$

where the reflection-symmetric controls are illustrated in Figure 1 (a) without the green control fields. Next, we introduce an additional control term H_{break} that breaks the lattice reflection symmetry. As illustrated in Figure 1(a), an example is a global field (shown in green) that acts on only half of the system. The specific form of H_{break} is not important—it could represent interactions, local rotations, or other types of controls. As detailed in Appendix B, H_{break} decouples all qubits with their mirror pairs, thereby generating the universal gate set as:

$$\text{span}_{\mathbb{R}}\langle iH_X, iH_Z, iH_{ZZ}, iH_{\text{break}} \rangle_{\text{Lie}} = \text{span}_{\mathbb{R}}\langle \cup_j iX_j, \cup_j iZ_j, \cup_j iZ_j Z_{j+1} \rangle_{\text{Lie}}, \quad (4)$$

which demonstrates the sufficiency part in Theorem 1. The necessity part is straightforward, as the reflection symmetry will decompose the Hilbert space into different sectors, which prohibits universal quantum computation.

Theorem 1 is general in various senses. First, the theorem illustrates the connection between geometrical symmetry breaking and universal quantum computation. The one-dimensional proof is generalizable to any higher-dimensional lattice, or even to a general graph (see discussion in Appendix B), and we leave the detailed proof for future study. Second, our theorem includes previous studies as special cases. The proofs of universality for globally controlled quantum dots [36] and QAOA [37] both require the qubits to form an even-odd alternating, dual-species pattern like $ABAB\dots$. Then, the following control Hamiltonians, supported on either one species or both, can realize universal quantum computation:

$$H_1 = \sum_j X_j, \quad H_A = \sum_j Z_{2j}, \quad H_B = \sum_j Z_{2j+1}, \quad H_{AB} = \sum_j Z_{2j} Z_{2j+1}, \quad H_{BA} = \sum_j Z_{2j+1} Z_{2j+2}. \quad (5)$$

Compared to Equation (2), we find the equivalence $H_X = H_1$, $H_Z = H_A + H_B$, and $H_{ZZ} = H_{AB} + H_{BA}$. Therefore, the control structure in Equation (5) is included in Theorem 1, with two specific additional symmetry-breaking terms $H_{\text{break}1} = \sum_j Z_{2j}$ and $H_{\text{break}2} = \sum_j Z_{2j} Z_{2j+1}$. Notably, this structure turns out to be convenient in current dual-species neutral atom platforms [66], which further demonstrates the applicability of our theorem.

B. Extension to fermions and bosons

We generalize the above idea to fermionic and bosonic systems, focusing on the experimental platform of ultracold atoms in optical superlattices. Building upon standard optical lattices, superlattices introduce a double periodicity

in the optical trapping potential and have recently shown great promise for simulating fermionic and bosonic systems—enabling applications such as quantum chemistry simulations [39] and the engineering of next-nearest-neighbor couplings in the Hubbard model [41]. Despite this experimental progress, the fundamental capabilities and limitations of such globally controlled platforms remain unclear. Here, we show that these systems are surprisingly powerful and capable of universal fermionic and bosonic quantum simulation.

For fermionic and bosonic simulations, a set of physical controls is termed universal if it can generate the entire unitary group acting on the corresponding Hilbert space. Experimentally, all relevant physical operations preserve particle number, so we can restrict our analysis to fixed-particle-number Hilbert spaces of fermions and bosons, denoted by \mathcal{H}_f and \mathcal{H}_b , respectively. By Theorems 2 and 3 of Ref. [67], free fermion/boson operations plus a uniform Hubbard-type interaction generate all unitaries in $\mathcal{H}_f/\mathcal{H}_b$, so it suffices to consider the realization of those controls.

For simplicity, we focus on a one-dimensional optical superlattice with spinless fermions or bosons, and the generalization to higher-dimensional superlattices and spinful particles is straightforward (see discussions in Appendix C). We use c_i^\dagger and c_i to denote the fermionic/bosonic creation and annihilation operators at site i , respectively, and the corresponding particle number operator is denoted by $n_i = c_i^\dagger c_i$. The uniform Hubbard interaction is given by $H_U = \sum_j n_j n_{j+1}$. Moreover, the double periodicity in the optical trapping potential enables us to control the hopping and chemical potential terms globally in an even-odd alternating pattern. This yields the following basic control Hamiltonians: $H_{\text{even}}^{(\text{hop})} = \sum_j (c_{2j}^\dagger c_{2j+1} + \text{h.c.})$, $H_{\text{odd}}^{(\text{hop})} = \sum_j (c_{2j+1}^\dagger c_{2j+2} + \text{h.c.})$, $H_{\text{even}}^{(\mu)} = \sum_j n_{2j}$, and $H_{\text{odd}}^{(\mu)} = \sum_j n_{2j+1}$. Therefore, the system is described by:

$$H(t) = -J_{\text{even}}(t)H_{\text{even}}^{(\text{hop})} - J_{\text{odd}}(t)H_{\text{odd}}^{(\text{hop})} + \mu_{\text{even}}(t)H_{\text{even}}^{(\mu)} + \mu_{\text{odd}}(t)H_{\text{odd}}^{(\mu)} + UH_U, \quad (6)$$

where $J_{\text{even/odd}}(t)$ and $\mu_{\text{even/odd}}(t)$ are the corresponding time-dependent control pulses.

As discussed earlier, to prove universality, provided the uniform Hubbard interaction H_U , it suffices to demonstrate that the other control Hamiltonians in Equation (6) can generate all free fermion/boson operations. To achieve that, as detailed in Appendix C, we first show that they realize the independent control over nearest-neighbor hopping and on-site chemical potential terms, as given by:

$$\text{span}_{\mathbb{R}} \langle iH_{\text{even}}^{(\text{hop})}, iH_{\text{odd}}^{(\text{hop})}, iH_{\text{even}}^{(\mu)}, iH_{\text{odd}}^{(\mu)} \rangle_{\text{Lie}} = \text{span}_{\mathbb{R}} \langle \cup_j i(c_j^\dagger c_{j+1} + \text{h.c.}), \cup_j i n_j \rangle_{\text{Lie}}. \quad (7)$$

Then, using Lemma 9 in Appendix C, we equate the DLA on the right-hand side of Equation (7) to that of free operations, which completes the proof (see Theorems 8 and 11).

For spinful particles, the spin degree of freedom can be treated as two internal modes. Using a similar method (see Theorem 12), we show that two additional control fields are required to achieve universality: (1) a uniform global spin- X magnetic field and (2) a global spin- Z magnetic field with a linear gradient. These extend the previously established universal control set for two-site systems to the full optical superlattice [68].

In summary, our results on universal quantum simulation provide a rigorous foundation for leveraging optical superlattices to explore complex fermionic and bosonic phenomena, with potential applications in quantum chemistry and condensed matter physics. As an illustrative example, we consider the simulation of the two-dimensional Fermi-Hubbard model with next-nearest-neighbor (NNN) hoppings—widely regarded as a promising candidate for realizing high-temperature superconductivity [69–72]—as detailed in Appendix D. We anticipate that our framework sets the stage for ultracold atom platforms to probe richer quantum phenomena in both fundamental and applied contexts.

III. ENGINEERED THREE-BODY INTERACTION AND TOPOLOGICAL DYNAMICS

Building on our theoretical framework, we demonstrate that globally-controlled analog simulators can realize effective Hamiltonians far beyond their native physical interactions through pulse engineering [Figure 1(b)]. In this section, we showcase this potential by experimentally engineering a three-body interacting Hamiltonian using Rydberg atom arrays as illustrated in Figure 1(c). To our knowledge, this is the first realization of effective three-body interactions with Rydberg atoms outside the blockade regime, going beyond the native two-body interactions. Crucially, we introduce a new control technique, dubbed *direct quantum optimal control*, that bridges the gap between theoretical possibility and experimental reality. This method enables us to overcome key experimental challenges, including hardware constraints and atom position fluctuations outside the blockade regime, by identifying smooth, short-duration pulses that achieve high-fidelity dynamics. In the following, we introduce the physics model of interest, which has a topological phase, and describe its implementation using Rydberg atom arrays.

A. Example application: symmetry-protected topological phases

Topology has emerged as a cornerstone of modern quantum many-body physics. Topological phases are typically characterized by non-local order parameters and topological edge modes localized at the system boundaries [51, 73, 74]. In one-dimensional systems, such a topological phase is well defined in the presence of symmetries, giving rise to symmetry-protected topological (SPT) phases [51, 75–77]. With the development of programmable quantum devices, researchers have begun experimentally investigating exotic topological phases of matter, ranging from preparing topological quantum states [52, 78] to exploring topological phases and transitions [31, 79, 80], Floquet topological dynamics [81, 82], and anyon statistics [83–85]. Most of these demonstrations and proposals have relied on digital quantum circuits.

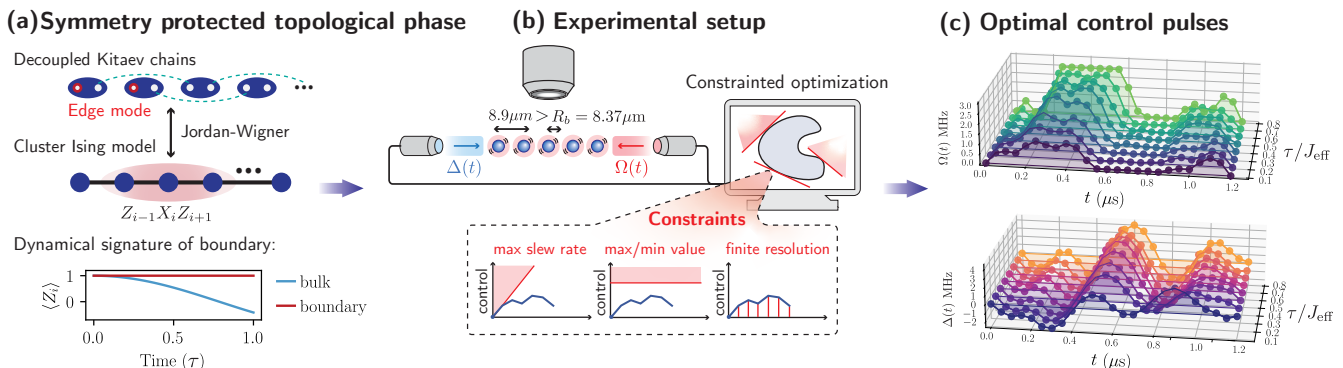


FIG. 2. **Experimental realization of symmetry-protected topological dynamics using optimal control.** (a) Symmetry-protected topological Hamiltonian. A pair of decoupled Kitaev chains, which host topological edge modes, can be mapped to a qubit model with three-body interactions known as the cluster-Ising model. Due to experimental constraints, only measurements in the Z-basis are available. A key dynamical signature distinguishing boundary from bulk qubits is that the Z expectation values of the boundary qubits remain unchanged under evolution with the ZXZ Hamiltonian. (b) Schematic of the experimental setup. Rydberg atom arrays are globally driven by time-dependent Rabi frequency $\Omega(t)$ and detuning $\Delta(t)$. Atoms are spaced beyond the blockade radius R_b [86], resulting in position fluctuations due to residual atomic temperature. Optimal quantum control is employed to design global pulses that mitigate errors and also satisfies machine constraints. (c) Overview of optimal control pulses used in the experiments. Time-dependent control waveforms $\Omega(t)$ and $\Delta(t)$ are engineered to simulate the effective SPT Hamiltonian. Constraints such as maximum slew rate, amplitude bounds, and finite time resolution are incorporated in the control optimization.

In parallel, there has been significant progress in analog quantum devices and digital-analog hybrid platforms. By avoiding the discretization errors introduced by Trotterization, analog and hybrid devices offer improved simulation quality, especially for quantum dynamics [19, 87, 88]. Notably, Ref. [31] demonstrated a bosonic version of the SPT model using Rydberg atom arrays. However, including this demonstration, most analog quantum simulations still relied heavily on the native Hamiltonians of the device and primarily focused on engineered two-body interactions. Building on the theoretical framework we developed, we show that the expressive power of analog quantum devices is significantly greater. These systems can simulate broad classes of exotic Hamiltonians that go well beyond their native two-body interactions. For example, with global pulse engineering, one can in principle engineer multi-body interactions. In this work, we demonstrate the quantum dynamics driven by an effective ZXZ Hamiltonian (also called cluster-Ising model):

$$H_{\text{ZXZ}} = J_{\text{eff}} \sum_j Z_{j-1} X_j Z_{j+1}, \quad (8)$$

which also serves as a pedagogical example of a system realizing a symmetry-protected topological (SPT) phase. Through the Jordan-Wigner transformation, this model can be mapped to a pair of decoupled Kitaev chains [51, 89], supporting a topological edge mode, as illustrated in Figure 2(a) (see Appendix E for details). Although both the cluster-Ising model and the bosonic Su–Schrieffer–Heeger model in Ref. [31] are SPT Hamiltonians, our work highlights the potential to engineer multi-body interactions beyond the native interactions of the hardware.

In particular, we use the platform of Rydberg atoms trapped in a tweezer array where a qubit is encoded as the ground and Rydberg states of the atom. As illustrated in Figure 2(b), the atoms are placed outside the blockade region [86] and globally driven by time-dependent Rabi frequency $\Omega(t)$ and detuning $\Delta(t)$, which serves the role of

$u_\alpha(t)$ in Equation (1). The goal is to find experimentally feasible control pulses $u_\alpha^{(\tau)}(t)$ such that

$$\mathcal{T} \left[e^{-i \int dt \sum_\alpha u_\alpha^{(\tau)}(t) H_\alpha} \right] = e^{-i\tau H_{\text{Zxz}}}, \quad (9)$$

realizing the target unitary evolution under the cluster-Ising Hamiltonian, where the control pulse $\mathbf{u}^{(\tau)}(t)$ also depends on the effective simulation time τ .

Several key experimental challenges must be overcome to achieve this goal. As illustrated in Figure 2(b), the laser control parameters $\Omega(t)$ and $\Delta(t)$ are constrained by maximum slew rates, bounded amplitudes, and finite time discretization. These limitations make the optimization problem non-convex and challenging for traditional quantum control methods. Moreover, since the atoms are not trapped during evolution (see Section IV), long pulse durations inevitably lead to deviations from ideal dynamics. Thus, it is essential to design smooth, short-duration control pulses. To achieve this, we introduce a new quantum control method adapted from a cutting-edge robotics technique called direct trajectory optimization and benchmark it against standard approaches. This method successfully identifies a family of smooth pulses, as shown in Figure 2(c), that achieve the experimental target defined in Equation (9), where traditional methods fail.

B. Experimental setup and Rydberg atom arrays

The physical platform we use is a neutral atom array trapped in optical tweezers designed by QuEra Computing [90]. Qubits are encoded in the electronic ground state $|g\rangle = |5S_{1/2}\rangle$ as $|0\rangle$ and in the Rydberg excited state $|r\rangle = |70S_{1/2}\rangle$ as $|1\rangle$ of the ^{87}Rb atom. Transitions between these states are driven by a two-photon process using laser beams at 420 nm and 1013 nm, while the atoms interact via van der Waals interactions between Rydberg states. The full control Hamiltonian is given by

$$H(t)/\hbar = \frac{\Omega(t)}{2} \sum_l (|g_l\rangle\langle r_l| + |r_l\rangle\langle g_l|) - \Delta(t) \sum_l |r_l\rangle\langle r_l| + \sum_{j<l} V_{jl} |r_j\rangle\langle r_j| \otimes |r_l\rangle\langle r_l|, \quad (10)$$

where $\Omega(t)$ is the global Rabi frequency, $\Delta(t)$ is the global detuning, $V_{jl} = C_6/|\vec{x}_j - \vec{x}_l|^6$ describes the van der Waals interaction between atoms j and l , with $C_6 = 862,690 \times 2\pi \text{ MHz}\cdot\mu\text{m}^6$ and \hbar is the reduced Planck's constant. With the qubit encoding described above, this Hamiltonian closely resembles a transverse-field Ising model with long-range, algebraically decaying interactions.

This qubit encoding is commonly referred to as the analog mode of Rydberg atom arrays, in contrast to the digital mode, which encodes qubits in two hyperfine ground states [6, 91, 92]. In the analog mode, atoms are initially trapped in their ground states but become untrapped once global control pulses excite them to Rydberg states. The residual thermal motion causes fluctuations in atomic positions, which in turn lead to decoherence through Rydberg state decay. As a result, most analog quantum simulations with Rydberg atom arrays have been performed within the blockade regime [52, 53], where neighboring atoms are separated by less than the blockade radius $R_b = (C_6/\Omega_{\text{max}})^{1/6}$ [54, 55, 86]. In the blockade regime, the nearest-neighbor interactions are much stronger than the Rabi frequency. Therefore, simultaneous excitations of neighboring atoms are suppressed and nearest-neighbor interactions are effectively eliminated. This configuration is more robust to atom position fluctuations.

However, using the theoretical tools we developed, we show that although the three-body ZXZ Hamiltonian cannot be engineered within the typical blockade regime, H_{ZXZ} can be realized outside it (see Appendix E1). In our experiment, the maximum Rabi frequency is $\Omega_{\text{max}} = 2.4 \text{ MHz}$, yielding a blockade radius of $R_b = 8.37 \mu\text{m}$. We arrange atoms in a one-dimensional chain with a spacing of $d = 8.9 \mu\text{m}$, just outside the blockade radius.

Achieving this goal requires overcoming several key experimental challenges. The first is the decoherence error from the finite residual temperature of the atoms. As we will discuss in later sections, this noise source can be effectively mitigated by designing short-duration control pulses, without modifying the hardware. In addition to thermal motion, we must also respect strict constraints on the laser control parameters, as detailed in Appendix H. These combined challenges call for the design of global control pulses that satisfy all experimental constraints, are smooth, and remain short in duration to minimize decoherence. Together, these factors highlight the experimental complexity and the need for fine-tuned quantum optimal control.

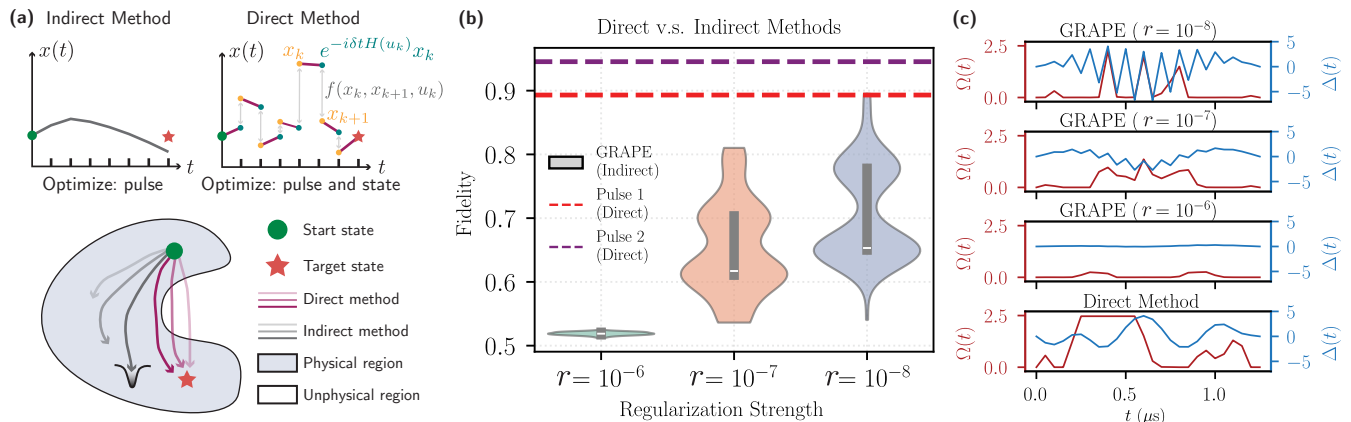


FIG. 3. **Comparison between direct and indirect quantum optimal control methods.** (a) Schematic illustration of indirect v.s. direct quantum optimal control. The indirect method (left) optimizes only the control pulses \mathbf{u}_k , with intermediate states x_k determined solely by the Schrödinger equation. In contrast, the direct method (right) simultaneously optimizes both the control pulses and intermediate states, treating the Schrödinger equation as a constraint — allowing traversal of unphysical regions during optimization (visualized as discrete jumps in state space). Therefore, they explore different loss landscape during optimization as shown in the lower panel. (b) Comparison of final unitary fidelities achieved by GRAPE (indirect) and the direct method, targeting an effective evolution time $\tau/J_{\text{eff}} = 0.8$ under realistic machine constraints. GRAPE results are shown for three regularization strengths r that penalize the second derivative to impose pulse smoothness. For each r , 100 GRAPE runs with random initializations are shown as violin plots; the thick bar marks the interquartile range and the white marker indicates the median. Two smooth pulse control obtained from the direct method (Pulse 1 with $T = 1.2\mu\text{s}$ and Pulse 2 with $T = 3.6\mu\text{s}$) are marked for comparison. (c) Typical examples of optimized pulses for Rabi frequency $\Omega(t)$ (MHz) and detuning $\Delta(t)$ (MHz) using GRAPE and the direct method (Pulse 1).

C. Direct Quantum Optimal Control

To tackle these difficulties, we introduce a new quantum optimal control approach, dubbed *direct quantum optimal control* (direct method hereafter), inspired by the direct trajectory optimization technique from robotics [42]. As we will demonstrate later in this section, this method explores a fundamentally different loss landscape compared to conventional quantum control techniques, making it particularly effective in the presence of stringent hardware constraints where other methods often fail.

In quantum optimal control (QOC), we start with the unitary propagator $U(t=0) = I_{2N}$. It evolves according to Schrödinger equation

$$\frac{\partial U}{\partial t} = -iH[\mathbf{u}(t)]U, \quad (11)$$

where $\mathbf{u}(t)$ represents the control pulse trajectory. The goal of QOC is to find an optimal $\mathbf{u}(t)$, $t \in [0, T]$ such that $U(T)$ can approximate a target unitary U_{target} while satisfying hardware constraints. We discretize the time interval $[0, T]$ into n steps with duration δt and denote the unitary propagator and control parameters at the k -th time step by U_k and \mathbf{u}_k , respectively. Then, the QOC problem can be expressed as the following optimization problem:

$$\text{maximize } \mathcal{F}(U_n, U_{\text{target}}) \quad (12a)$$

$$\{\mathbf{u}_k\}_{k=1}^n$$

$$\text{subject to } U_n = \prod_{k=1}^n \exp[-iH(\mathbf{u}_k)\delta t] \quad (12b)$$

where the objective function is the unitary fidelity, denoted \mathcal{F} , between U_n and U_{target} . A widely used approach for solving this type of optimization problem is the Gradient Ascent Pulse Engineering (GRAPE) method [50]. For an initial guess of the control pulse $\mathbf{u}(t)$, one can evaluate the gradient $\partial\mathcal{F}(U_n, U_{\text{target}})/\partial\mathbf{u}_k$ with respect to pulse control parameters and then use the gradient ascent method to refine it iteratively. This workflow is illustrated on the left side and lower panel of Figure 3(a). In the optimal control literature, this strategy is commonly known as *indirect shooting method* [93].

While GRAPE performs well in relatively simple settings without control constraints, we find that it struggles when hardware constraints are introduced and is often prone to getting trapped in local minima. In contrast, aerospace and

robotics researchers have developed alternative techniques known as *direct methods* [94, 95], which reformulate the above optimization in a fundamentally different way: Instead of using the Schrödinger dynamics in Equation (11) to compute the unitary evolution U_n across time steps $[t_1, t_2, \dots, t_n]$, the Schrödinger equation is treated as an additional constraint, and the intermediate unitary operators U_k at each time step are augmented as trainable parameters (also called decision variables in robotics). Specifically, the above optimization problem is rewritten as the following constrained nonlinear program:

$$\begin{aligned} & \underset{\{\mathbf{u}_k, U_k\}_{k=1}^n}{\text{maximize}} && \mathcal{F}(U_n, U_{\text{target}}) \end{aligned} \quad (13a)$$

$$\text{subject to} \quad U_{k+1} = \exp[-iH(\mathbf{u}_k)\delta t]U_k, \quad \forall k \in \{1, \dots, n\}. \quad (13b)$$

Although it may appear to be a simple reformulation, the direct method explores a fundamentally different loss landscape compared to the indirect approach. In practice, the Schrödinger equation is enforced via Lagrange multipliers. The optimization can begin with an infeasible initial guess, allowing violations of the Schrödinger dynamics that manifest as discontinuities in $U(t)$, as shown in the right panel of Figure 3(a). This flexibility enables the optimizer to explore unphysical regions (e.g., unphysical jumps in $U(t)$), which can help with escaping local minima. This key distinction is further illustrated in the lower panel of Figure 3(a). Another advantage of the direct method is that the framework naturally handles any constraints on its trainable parameters, which include both states and controls. This feature is particularly useful for hardware experiments, where laser controls are subject to numerous technical limitations and durations should be kept as short as possible to limit decoherence.

We compared the performance of the direct method and GRAPE in synthesizing the unitary evolution generated by the ZZZ Hamiltonian for an effective time of $\tau/J_{\text{eff}} = 0.8$. Using the direct method, we explored two total pulse durations: $T = 1.2 \mu\text{s}$ and $T = 3.6 \mu\text{s}$ (we will justify these choices later). The shorter pulse, Pulse 1 (shown in Figure 3(b)), achieves a unitary fidelity of 89.4% on a three-atom chain, while the longer Pulse 2 yields a higher fidelity of 94.5% [96].

For GRAPE, we imposed the same hardware constraints using Lagrange multipliers and introduced an additional penalty term r on the second derivative of the control pulses to enforce smoothness. For each value of $r = 10^{-6}, 10^{-7}, 10^{-8}$, we performed 100 random initializations of the controls. Figure 3(b) shows the distribution of resulting unitary fidelities as violin plots, where the width reflects the density of solutions. Compared to GRAPE, the direct method achieves significantly higher fidelities, and GRAPE's performance is highly sensitive to the choice of r . Figure 3(c) shows typical control pulses found by both methods. For small r , GRAPE yields irregular control solutions, while slightly larger r jeopardizes the optimization, resulting in nearly flat pulses. In contrast, the direct method finds smooth, high-fidelity pulses that meet all experimental constraints. Further details are provided in Appendix G. In the next section, we implement the global control pulses (Pulse 1 and Pulse 2) in the experiment. As we will see, although Pulse 2 achieves higher unitary fidelity, its longer duration leads to increased decoherence, since the atoms are not trapped. In contrast, despite having lower unitary fidelity, the shorter Pulse 1 produces clearer topological edge signatures. This highlights that unitary fidelity can be an overly stringent metric, as analog simulations primarily focus on local observables, which tend to be more robust and better preserved than global quantities like unitary fidelity [87].

IV. EXPERIMENTAL RESULTS

In the experiments, we apply global laser controls $\Omega(t)$ and $\Delta(t)$ to a chain of atoms separated by $d = 8.9 \mu\text{m}$, slightly larger than the Rydberg blockade radius. The atoms are initially prepared in their ground states, trapped, and sorted into the desired configuration using optical tweezers. We use fluorescence imaging to preselect valid initial configurations and discard experimental runs in which atoms are not successfully imaged. In the current experimental setup [90], measurements are restricted to the Pauli- Z basis of each atom, corresponding to imaging the Rydberg density. With this constraint, our key observable is the stability of the boundary operators Z_L and Z_R , which correspond to the two edge qubits. Theoretically, they satisfy the commutation relations:

$$\begin{aligned} [Z_L, H_{\text{ZZXZ}}] &= [Z_R, H_{\text{ZZXZ}}] = 0, \\ [Z_L Z_R, H_{\text{ZZXZ}}] &= 0. \end{aligned} \quad (14)$$

This implies that the single-site Rydberg densities at the boundaries should remain constant during the evolution. Moreover, the persistence of stable correlations between the edge qubits, captured by the stability of $\langle Z_L Z_R \rangle$, serves as a dynamical signature of topological edge modes. We acknowledge this Z basis measurement constraint is a limitation in the current platform, which can be mitigated by future hardware improvements. For example, the digital-analog

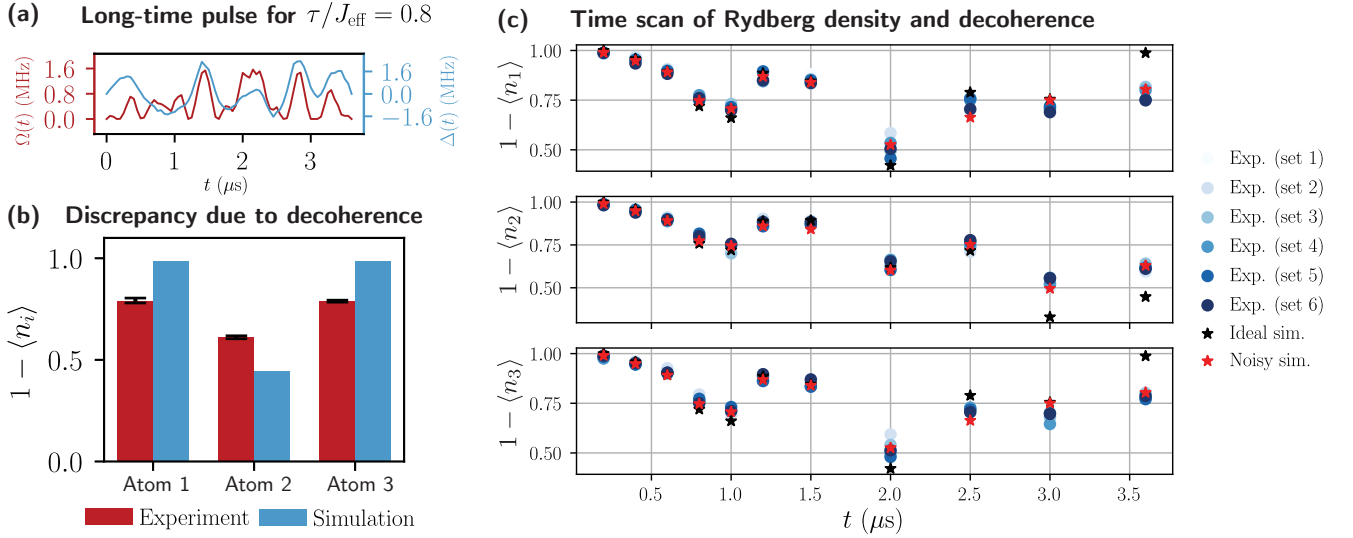


FIG. 4. **Characterizing noise in experiment using time-resolved Rydberg density.** (a) Control pulses ($\Omega(t)$ and $\Delta(t)$) obtained from the direct method (Pulse 2) targeting effective evolution time $\tau/J_{\text{eff}} = 0.8$. (b) Single-site Rydberg density ($1 - \langle n_i \rangle$) measured at the end of the pulse sequence for a three-atom chain initially prepared in the ground state. While the ideal unitary evolution predicts two peaks at atom 1 and atom 3, experimental results (red) deviate from the ideal simulation (blue), indicating the presence of noise. (c) Time-resolved scan of ($1 - \langle n_i \rangle$) for all three atoms during pulse application. Six separated three-atom clusters were measured in experiments in parallel (light to dark blue). Black stars indicate noiseless simulation results, and red stars represent noisy simulations incorporating Rydberg decay (incoherent error) and drifts in $\Omega(t)$ and $\Delta(t)$ (coherent error). The apparent deviation for $t > 1.5\mu\text{s}$ from ideal dynamics highlights the impact of realistic experimental imperfections. The size of the experimental error bars (standard deviation) is smaller than that of the markers.

Rydberg array platform [97, 98] may enable measurement in arbitrary bases through single-qubit rotations prior to readout.

Although longer pulse durations offer greater control flexibility and can generally achieve higher fidelities, they are not ideal in real experiments due to decoherence from Rydberg decay. In the previous section, we found two global control pulses (Pulse 1 and Pulse 2) that can synthesize the unitary evolution of the ZXZ Hamiltonian for an effective time of $\tau/J_{\text{eff}} = 0.8$. While Pulse 2 (shown in Figure 4(a)) achieves higher unitary fidelity, its experimental performance deviates from the ideal pulse simulation. As illustrated in Figure 4(b), ideal simulations on a three-atom chain predict high values of $1 - \langle n_i \rangle$ for the boundary atoms, whereas the experimental data show a clear decay from these ideal values. To better understand this discrepancy, we apply the global control pulse and measure the single-site Rydberg density of each atom at various intermediate time points. These results, shown as blue dots in Figure 4(c), reveal increasing deviation from the ideal pulse simulation (black stars) as time progresses.

This discrepancy between the experimental data and the ideal simulation for the long-duration pulse can be well explained by the following Lindblad error model:

$$\partial\rho/\partial t = -\frac{i}{\hbar}[H(t), \rho] + \sum_l \gamma_l \left(\sigma_l^- \rho \sigma_l^+ - \frac{1}{2} \{ \sigma_l^+ \sigma_l^-, \rho \} \right) \quad (15)$$

where the Lindblad operators σ_l^- capture Rydberg-state decay for each atom, caused by residual thermal motion (incoherent error). To account for coherent errors, we incorporate calibration offsets in the Rabi frequency $\Omega(t)$ and detuning $\Delta(t)$ of the Hamiltonian $H(t)$ (see Equation (10)):

$$\Delta_{\text{exp}}(t) = \Delta_{\text{input}}(t) + \delta\Delta, \quad \Omega_{\text{exp}}(t) = \Omega_{\text{input}}(t) + (\delta\Omega + k\Omega_{\text{input}}(t)), \quad (16)$$

where $\Delta_{\text{exp}}(t)$ and $\Omega_{\text{exp}}(t)$ are the experimentally realized values of detuning and Rabi frequency respectively; $\Delta_{\text{input}}(t)$ and $\Omega_{\text{input}}(t)$ are input control parameters; and $\delta\Delta$ and $\delta\Omega$ are constant shifts [99]. Using this error model, we find the best fit with $\gamma_l = 0.049$, $\delta\Delta = -0.049$ MHz, $\delta\Omega = -0.032$ MHz, and $k = -0.05$. The resulting noisy simulation (red stars in Figure 4(c)) shows good agreement with the experimental data and is consistent with our calibration experiments.

While the coherent errors in the model can be compensated by adjusting the input parameters, the most effective strategy to mitigate incoherent errors without modifying the hardware is to employ short-duration control pulses.

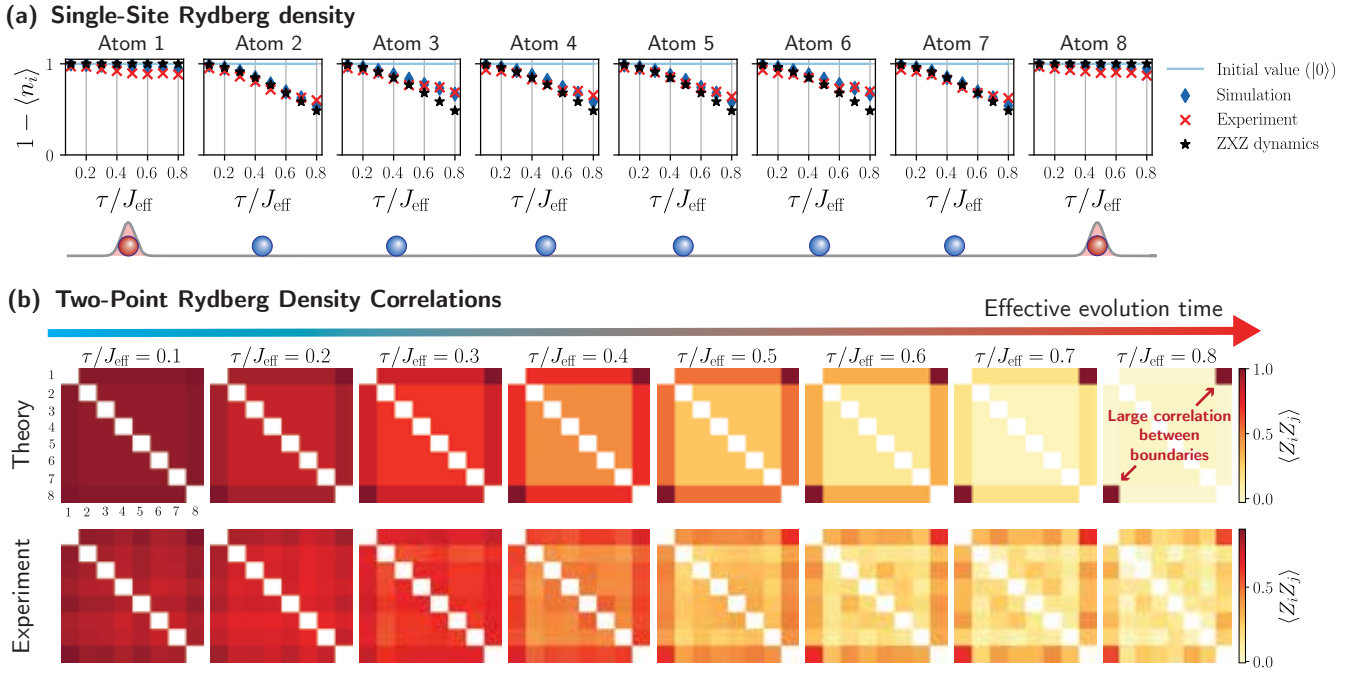


FIG. 5. **Experimental signatures of topological dynamics.** (a) Single-site Rydberg density after applying the optimized global pulse [see Figure 2(c)] to an 8-atom chain initialized in the ground state. Boundary atoms (1 and 8) retain high expectation values, while bulk atoms show decay with increasing τ/J_{eff} , which is consistent with edge mode behavior of the ZXZ Hamiltonian (black stars). Experimental results (red crosses) closely match ideal simulations (blue diamonds) due to short-time control pulses. (b) We measure connected two-point correlations $\langle Z_i Z_j \rangle$ between all pairs of atoms at different τ/J_{eff} . The top row shows theoretical predictions under ZXZ dynamics, which feature strong and persistent correlations between the boundary atoms. The bottom row presents experimental results, revealing similar edge correlations that reflect the presence of topological edge modes in the realized dynamics. The size of the experimental error bars (standard deviation) is smaller than that of the markers.

Indeed, Figure 4(c) shows that the experimental results closely match the ideal simulations when the pulse duration is shorter than $1.5 \mu\text{s}$. Based on this, we use the direct method to design a smooth control pulse with a total duration of $T = 1.2 \mu\text{s}$ (Pulse 1) for $\tau/J_{\text{eff}} = 0.8$. Starting from this pulse, we gradually construct smooth control pulses for $\tau/J_{\text{eff}} = 0.7, 0.6, \dots, 0.1$. This family of global control pulses is visualized in Figure 2(c).

We apply this family of global laser controls to a Rydberg atom array consisting of eight atoms, initialized in their ground states and arranged into the desired spatial configuration. After the system evolves under the control pulses, we measure the Rydberg density n_i (proportional to the Pauli-Z operator) and two-point correlations between all pairs of atoms using fluorescence imaging. As shown in Figure 5(a), the quantity $1 - \langle n_i \rangle$ exhibits behavior consistent with the theoretical predictions of topological SPT dynamics: the expectation values for the two boundary atoms remain stabilized, while those for the bulk atoms decay as the effective evolution time τ/J_{eff} increases. As for correlations, since $[Z_L Z_R, H_{\text{ZXZ}}] = 0$, the correlation between the two boundary atoms is expected to be stabilized. Since the system starts in a product state of ground states, strong correlations between the boundaries are expected to emerge and persist during the evolution under the ZXZ Hamiltonian. Our experimental results confirm this behavior, as shown in Figure 5(b), where the boundary correlations follow the signature given by theoretical predictions.

We acknowledge that, due to current hardware limitations, measurements are restricted to the Pauli-Z basis. Nonetheless, the above results provide strong evidence for the realization of the ZXZ Hamiltonian. In Appendix H, we present additional experimental data where an initial global control pulse is applied to drive the system from the ground state to a different initial state, followed by our main control pulse. These results also show good agreement with theoretical predictions. However, a drawback of this approach is that prepending an extra pulse increases the total experimental time and inevitably introduces additional noise due to atomic motion, which is not ideal.

In the future, we look forward to the expansion of hardware capabilities to enable measurements in arbitrary bases, allowing for full Hamiltonian learning [100–103] and direct verification of the effective Hamiltonian. Additionally, we envision integrating the direct optimal control loop with the hardware to enable real-time fine-tuning of control pulses to further enhance control fidelity, which we discuss in the Outlook. Despite current limitations, our experiment represents a significant first step toward synthesizing three-body interactions beyond the native hardware Hamiltonian

on analog quantum simulators using quantum optimal control. We anticipate that this work will inspire a wide range of future applications.

V. OUTLOOK

To fully realize the potential of programmable quantum simulators, we identify three key directions for future exploration: (1) efficient pulse-level calibration and noise learning, (2) large-scale quantum optimal control, and (3) robust analog quantum simulation. In experimental settings, control noise and pulse imperfections are unavoidable. While our current method accounts for known error models during optimization, unknown or drifting errors may still degrade performance. It is therefore important to develop tools that use our approach as a warm start for pulse design, while incorporating real-time experimental feedback to calibrate and refine control sequences on the fly. Such an online optimization strategy could benefit from randomized measurement protocols [102, 104, 105], which offer scalable quantum-classical data interfaces. These measurement results can also be used to infer effective Hamiltonians, enabling both improved pulse calibration and direct verification of synthesized interactions [100, 101, 103].

A second direction is the extension of our approach to large-scale quantum systems beyond classical simulation limits. For example, it would be valuable to engineer exotic Hamiltonians with multi-body interactions in two-dimensional systems. Several strategies could support this goal. Recent developments in classical simulation tools, such as Pauli propagation [106–108] and tensor network methods [109–112], enable efficient estimation of local observables in noisy, high-dimensional systems. Incorporating these tools into quantum optimal control frameworks could produce high-quality control pulses offline. Then, one can further refine them with online optimal control. Alternatively, machine learning models could be trained to learn the smooth extrapolation of optimal global pulses found on different small system sizes to larger system sizes [113]. Another promising approach is to adopt a divide-and-conquer strategy, in which control protocols optimized for small subsystems are combined to enable large-scale simulation [114].

Finally, although analog quantum simulation lacks the full protection of fault-tolerant architectures, it demonstrates inherent robustness for local observables [87]. Understanding the sensitivity of the new effective analog simulation scheme to noise remains an important direction. A natural question is whether ideas from quantum error correction can be incorporated into analog protocols to further enhance their resilience. Recent advances have shown that logical subspaces engineered via error detecting codes can suppress coherent errors by introducing a spectral gap between the analog subspace and higher-lying states [115]. As the gap increases, the system becomes more robust to coherent control errors, which resembles the threshold behavior of the quantum error correction. Extending such ideas to pulse-level control may offer a promising path toward scalable and noise-resilient analog quantum technologies.

From a quantum optimal control perspective, our approach to effective analog quantum simulation via variational global pulse control also raises fundamental theoretical questions. One key question is how to define and quantify the “distance” between a machine-native Hamiltonian and a desired target Hamiltonian [116–118]. While different native Hamiltonians may be capable of realizing the same target dynamics, the difficulty or overhead required can vary significantly. This notion of distance could help classify control Hamiltonians into equivalence classes under polynomial overhead. It also prompts the broader question of whether all universal Hamiltonians are equivalent in this sense.

We believe these new results will stimulate further discussions in quantum many-body physics, quantum optimal control, and quantum simulation.

VI. ACKNOWLEDGEMENTS

We would like to thank Hsin-Yuan (Robert) Huang, Nik O. Gjonbalaj, Muqing Xu, Majd Hamdan, Francisco Machado, Shengtao Wang, Jun Yang, Zhengwei Liu for helpful discussions. S.F.Y. and H.Y.H. thank DARPA through their IMPAQT Program (HR0011-23-3-0023) and DOE through the QUACQ program (DE-SC0025572). L.C. and A.J. were supported in part by the Army Research Office MURI Grant W911NF-20-1-0082. A.J.G. was supported by an appointment to the Intelligence Community Postdoctoral Research Fellowship Program at University of Chicago administered by Oak Ridge Institute for Science and Education (ORISE) through an interagency agreement between the U.S. Department of Energy and the Office of the Director of National Intelligence (ODNI).

Author contributions: H.Y.H. and S.F.Y. conceived the idea and designed the project. H.Y.H. and L.C. developed the theory, and L.C. proved the main theorems. H.Y.H. and A.M.G. set up and carried out the experiments, and A.M.G. processed the experimental data. A.T. and A.J.G. developed the pulse optimization tools. Z.M., F.T.C., A.J., and S.F.Y. supervised the project. All authors contributed equally to the writing of the manuscript.

VII. DATA AVAILABILITY

Source data are available for this paper. All other data supporting the plots within this paper and other study findings are available from the corresponding author upon reasonable request.

VIII. CODE AVAILABILITY

The code used in this study is available from the corresponding author upon request.

-
- [1] R. Acharya, D. A. Abanin, L. Aghababaie-Beni, I. Aleiner, T. I. Andersen, M. Ansmann, F. Arute, K. Arya, A. Asfaw, N. Astrakhantsev, J. Atalaya, R. Babbush, D. Bacon, B. Ballard, J. C. Bardin, J. Bausch, A. Bengtsson, A. Bilmes, S. Blackwell, S. Boixo, G. Bortoli, A. Bourassa, J. Bovaird, L. Brill, M. Broughton, D. A. Browne, B. Buchea, B. B. Buckley, D. A. Buell, T. Burger, B. Burkett, N. Bushnell, A. Cabrera, J. Campero, H.-S. Chang, Y. Chen, Z. Chen, B. Chiaro, D. Chik, C. Chou, J. Claes, A. Y. Cleland, J. Cogan, R. Collins, P. Conner, W. Courtney, A. L. Crook, B. Curtin, S. Das, A. Davies, L. De Lorenzo, D. M. Debroy, S. Demura, M. Devoret, A. Di Paolo, P. Donohoe, I. Drozdov, A. Dunsworth, C. Earle, T. Edlich, A. Eickbusch, A. M. Elbag, M. Elzouka, C. Erickson, L. Faoro, E. Farhi, V. S. Ferreira, L. F. Burgos, E. Forati, A. G. Fowler, B. Foxen, S. Ganjam, G. Garcia, R. Gasca, É. Genois, W. Jiang, C. Gidney, D. Gilboa, R. Gosula, A. G. Dau, D. Graumann, A. Greene, J. A. Gross, S. Habegger, J. Hall, M. C. Hamilton, M. Hansen, M. P. Harrigan, S. D. Harrington, F. J. H. Heras, S. Heslin, P. Heu, O. Higgott, G. Hill, J. Hilton, G. Holland, S. Hong, H.-Y. Huang, A. Huff, W. J. Huggins, L. B. Ioffe, S. V. Isakov, J. Iveland, E. Jeffrey, Z. Jiang, C. Jones, S. Jordan, C. Joshi, P. Juhas, D. Kafri, H. Kang, A. H. Karamlou, K. Kechedzhi, J. Kelly, T. Khaira, T. Khattar, M. Khezri, S. Kim, P. V. Klimov, A. R. Klots, B. Kobrin, P. Kohli, A. N. Korotkov, F. Kostritsa, R. Kothari, B. Kozlovskii, J. M. Kreikebaum, V. D. Kurilovich, N. Lacroix, D. Landhuis, T. Lange-Dei, B. W. Langley, P. Laptev, K.-M. Lau, L. Le Guevel, J. Ledford, J. Lee, K. Lee, Y. D. Lensky, S. Leon, B. J. Lester, W. Y. Li, Y. Li, A. T. Lill, W. Liu, W. P. Livingston, A. Locharla, E. Lucero, D. Lundahl, A. Lunt, S. Madhuk, F. D. Malone, A. Maloney, S. Mandrà, J. Manyika, L. S. Martin, O. Martin, S. Martin, C. Maxfield, J. R. McClean, M. McEwen, S. Meeks, A. Megrant, X. Mi, K. C. Miao, A. Mieszala, R. Molavi, S. Molina, S. Montazeri, A. Morvan, R. Movassagh, W. Mruczkiewicz, O. Naaman, M. Neeley, C. Neill, A. Nersisyan, H. Neven, M. Newman, J. H. Ng, A. Nguyen, M. Nguyen, C.-H. Ni, M. Y. Niu, T. E. O'Brien, W. D. Oliver, A. Opremcak, K. Ottosson, A. Petukhov, A. Pizzuto, J. Platt, R. Potter, O. Pritchard, L. P. Pryadko, C. Quintana, G. Ramachandran, M. J. Reagor, J. Redding, D. M. Rhodes, G. Roberts, E. Rosenberg, E. Rosenfeld, P. Roushan, N. C. Rubin, N. Saei, D. Sank, K. Sankaragomathi, K. J. Satzinger, H. F. Schurkus, C. Schuster, A. W. Senior, M. J. Shearn, A. Shorter, N. Shutty, V. Shvarts, S. Singh, V. Sivak, J. Skrzny, S. Small, V. Smelyanskiy, W. C. Smith, R. D. Somma, S. Springer, G. Sterling, D. Strain, J. Suchard, A. Szasz, A. Szein, D. Thor, A. Torres, M. M. Torunbalci, A. Vaishnav, J. Vargas, S. Vdovichev, G. Vidal, B. Villalonga, C. V. Heidweiller, S. Waltman, S. X. Wang, B. Ware, K. Weber, T. Weidel, T. White, K. Wong, B. W. K. Woo, C. Xing, Z. J. Yao, P. Yeh, B. Ying, J. Yoo, N. Yosri, G. Young, A. Zalcman, Y. Zhang, N. Zhu, N. Zobrist, G. Q. AI, and Collaborators, *Nature* **638**, 920 (2025).
- [2] C. Ryan-Anderson, N. C. Brown, M. S. Allman, B. Arkin, G. Asa-Attuah, C. Baldwin, J. Berg, J. G. Bohnet, S. Braxton, N. Burdick, J. P. Campora, A. Chernoguzov, J. Esposito, B. Evans, D. Francois, J. P. Gaebler, T. M. Gatterman, J. Gerber, K. Gilmore, D. Gresh, A. Hall, A. Hankin, J. Hostetter, D. Lucchetti, K. Mayer, J. Myers, B. Neyenhuis, J. Santiago, J. Sedlacek, T. Skripka, A. Slattery, R. P. Stutz, J. Tait, R. Tobey, G. Vittorini, J. Walker, and D. Hayes, *arXiv e-prints*, [arXiv:2208.01863](https://arxiv.org/abs/2208.01863) (2022), [arXiv:2208.01863](https://arxiv.org/abs/2208.01863) [quant-ph].
- [3] D. Bluvstein, S. J. Evered, A. A. Geim, S. H. Li, H. Zhou, T. Manovitz, S. Ebadi, M. Cain, M. Kalinowski, D. Hangleiter, J. P. Bonilla Ataides, N. Maskara, I. Cong, X. Gao, P. Sales Rodriguez, T. Karolyshyn, G. Semeghini, M. J. Gullans, M. Greiner, V. Vuletić, and M. D. Lukin, *Nature* **626**, 58 (2024).
- [4] H. Putterman, K. Noh, C. T. Hann, G. S. MacCabe, S. Aghaeimeibodi, R. N. Patel, M. Lee, W. M. Jones, H. Moradinejad, R. Rodriguez, N. Mahuli, J. Rose, J. C. Owens, H. Levine, E. Rosenfeld, P. Reinhold, L. Monceli, J. A. Alcid, N. Alidoust, P. Arrangoiz-Arriola, J. Barnett, P. Bienias, H. A. Carson, C. Chen, L. Chen, H. Chinkejian, E. M. Chisholm, M.-H. Chou, A. Clerk, A. Clifford, R. Cosmic, A. V. Curiel, E. Davis, L. DeLorenzo, J. M. D'Ewart, A. Diky, N. D'Souza, P. T. Dumitrescu, S. Eisenmann, E. Elkhoully, G. Evenbly, M. T. Fang, Y. Fang, M. J. Fling, W. Fon, G. Garcia, A. V. Gorshkov, J. A. Grant, M. J. Gray, S. Grimberg, A. L. Grimsmo, A. Haim, J. Hand, Y. He, M. Hernandez, D. Hover, J. S. C. Hung, M. Hunt, J. Iverson, I. Jarrige, J.-C. Jaskula, L. Jiang, M. Kalaei, R. Karabalin, P. J. Karalekas, A. J. Keller, A. Khalajhedayati, A. Kubica, H. Lee, C. Leroux, S. Lieu, V. Ly, K. V. Madrigal, G. Marcaud, G. McCabe, C. Miles, A. Milsted, J. Minguzzi, A. Mishra, B. Mukherjee, M. Naghiloo, E. Oblepias, G. Ortuno, J. Pagdilao, N. Pancotti, A. Panduro, J. Paquette, M. Park, G. A. Pairs, D. Perello, E. C. Peterson, S. Ponte, J. Preskill, J. Qiao, G. Refael, R. Resnick, A. Retzker, O. A. Reyna, M. Runyan, C. A. Ryan, A. Sahmoud, E. Sanchez, R. Sanil, K. Sankar, Y. Sato, T. Scaffidi, S. Siavoshi, P. Sivarajah, T. Skogland, C.-J. Su, L. J. Swenson, S. M. Teo, A. Tomada, G. Torlai, E. A. Wollack, Y. Ye, J. A. Zerrudo, K. Zhang, F. G. S. L. Brandão, M. H. Matheny, and O. Painter, *Nature* **638**, 927 (2025).

- [5] V. V. Sivak, A. Eickbusch, B. Royer, S. Singh, I. Tsioutsios, S. Ganjam, A. Miano, B. L. Brock, A. Z. Ding, L. Frunzio, S. M. Girvin, R. J. Schoelkopf, and M. H. Devoret, *Nature* **616**, 50 (2023).
- [6] S. J. Evered, D. Bluvstein, M. Kalinowski, S. Ebadi, T. Manovitz, H. Zhou, S. H. Li, A. A. Geim, T. T. Wang, N. Maskara, H. Levine, G. Semeghini, M. Greiner, V. Vuletić, and M. D. Lukin, *Nature* **622**, 268 (2023).
- [7] H. Levine, A. Keesling, G. Semeghini, A. Omran, T. T. Wang, S. Ebadi, H. Bernien, M. Greiner, V. Vuletić, H. Pichler, and M. D. Lukin, *Phys. Rev. Lett.* **123**, 170503 (2019).
- [8] C. M. Löschnauer, J. Mosca Toba, A. C. Hughes, S. A. King, M. A. Weber, R. Srinivas, R. Matt, R. Nourshargh, D. T. C. Allcock, C. J. Ballance, C. Matthiesen, M. Malinowski, and T. P. Harty, *arXiv e-prints*, [arXiv:2407.07694](https://arxiv.org/abs/2407.07694) (2024), [arXiv:2407.07694](https://arxiv.org/abs/2407.07694) [quant-ph].
- [9] N.-C. Chiu, E. C. Trapp, J. Guo, M. H. Abobeih, L. M. Stewart, S. Hollerith, P. Stroganov, M. Kalinowski, A. A. Geim, S. J. Evered, S. H. Li, L. M. Peters, D. Bluvstein, T. T. Wang, M. Greiner, V. Vuletić, and M. D. Lukin, *arXiv e-prints*, [arXiv:2506.20660](https://arxiv.org/abs/2506.20660) (2025), [arXiv:2506.20660](https://arxiv.org/abs/2506.20660) [quant-ph].
- [10] H. J. Manetsch, G. Nomura, E. Bataille, K. H. Leung, X. Lv, and M. Endres, *arXiv e-prints*, [arXiv:2403.12021](https://arxiv.org/abs/2403.12021) (2024), [arXiv:2403.12021](https://arxiv.org/abs/2403.12021) [quant-ph].
- [11] S. A. Guo, Y. K. Wu, J. Ye, L. Zhang, W. Q. Lian, R. Yao, Y. Wang, R. Y. Yan, Y. J. Yi, Y. L. Xu, B. W. Li, Y. H. Hou, Y. Z. Xu, W. X. Guo, C. Zhang, B. X. Qi, Z. C. Zhou, L. He, and L. M. Duan, *Nature* **630**, 613 (2024).
- [12] G. Semeghini, H. Levine, A. Keesling, S. Ebadi, T. T. Wang, D. Bluvstein, R. Verresen, H. Pichler, M. Kalinowski, R. Samajdar, A. Omran, S. Sachdev, A. Vishwanath, M. Greiner, V. Vuletić, and M. D. Lukin, *Science* **374**, 1242 (2021), <https://www.science.org/doi/pdf/10.1126/science.abi8794>.
- [13] J. G. Bohnet, B. C. Sawyer, J. W. Britton, M. L. Wall, A. M. Rey, M. Foss-Feig, and J. J. Bollinger, *Science* **352**, 1297 (2016), <https://www.science.org/doi/pdf/10.1126/science.aad9958>.
- [14] P. Scholl, M. Schuler, H. J. Williams, A. A. Eberharter, D. Barredo, K.-N. Schymik, V. Lienhard, L.-P. Henry, T. C. Lang, T. Lahaye, A. M. Läuchli, and A. Browaeys, *Nature* **595**, 233 (2021).
- [15] M. Kornjača, H.-Y. Hu, C. Zhao, J. Wurtz, P. Weinberg, M. Hamdan, A. Zhdanov, S. H. Cantu, H. Zhou, R. Araiza Bravo, K. Bagnall, J. I. Basham, J. Campo, A. Choukri, R. DeAngelo, P. Frederick, D. Haines, J. Hammett, N. Hsu, M.-G. Hu, F. Huber, P. N. Jepsen, N. Jia, T. Karolyshyn, M. Kwon, J. Long, J. Lopatin, A. Lukin, T. Macri, O. Marković, L. A. Martínez-Martínez, X. Meng, E. Ostroumov, D. Paquette, J. Robinson, P. Sales Rodriguez, A. Singh, N. Sinha, H. Thoreen, N. Wan, D. Waxman-Lenz, T. Wong, K.-H. Wu, P. L. S. Lopes, Y. Boger, N. Gemelke, T. Kitagawa, A. Keesling, X. Gao, A. Bylinskii, S. F. Yelin, F. Liu, and S.-T. Wang, *arXiv e-prints*, [arXiv:2407.02553](https://arxiv.org/abs/2407.02553) (2024), [arXiv:2407.02553](https://arxiv.org/abs/2407.02553) [quant-ph].
- [16] T. Manovitz, S. H. Li, S. Ebadi, R. Samajdar, A. A. Geim, S. J. Evered, D. Bluvstein, H. Zhou, N. U. Koyluoglu, J. Feldmeier, P. E. Dolgirev, N. Maskara, M. Kalinowski, S. Sachdev, D. A. Huse, M. Greiner, V. Vuletić, and M. D. Lukin, *Nature* **638**, 86 (2025).
- [17] T. Hartke, B. Oreg, C. Turnbaugh, N. Jia, and M. Zwierlein, *Science* **381**, 82 (2023), <https://www.science.org/doi/pdf/10.1126/science.ade4245>.
- [18] T. I. Andersen, N. Astrakhantsev, A. H. Karamlou, J. Berndtsson, J. Motruk, A. Szasz, J. A. Gross, A. Schuckert, T. Westerhout, Y. Zhang, E. Forati, D. Rossi, B. Kobrin, A. D. Paolo, A. R. Klots, I. Drozdov, V. Kurilovich, A. Petukhov, L. B. Ioffe, A. Elben, A. Rath, V. Vitale, B. Vermersch, R. Acharya, L. A. Beni, K. Anderson, M. Ansmann, F. Arute, K. Arya, A. Asfaw, J. Atalaya, B. Ballard, J. C. Bardin, A. Bengtsson, A. Bilmes, G. Bortoli, A. Bourassa, J. Bovaird, L. Brill, M. Broughton, D. A. Browne, B. Buchea, B. B. Buckley, D. A. Buell, T. Burger, B. Burkett, N. Bushnell, A. Cabrera, J. Campero, H. S. Chang, Z. Chen, B. Chiaro, J. Claes, A. Y. Cleland, J. Cogan, R. Collins, P. Conner, W. Courtney, A. L. Crook, S. Das, D. M. Debroy, L. D. Lorenzo, A. D. T. Barba, S. Demura, P. Donohoe, A. Dunsworth, C. Earle, A. Eickbusch, A. M. Elbag, M. Elzouka, C. Erickson, L. Faoro, R. Fatemi, V. S. Ferreira, L. F. Burgos, A. G. Fowler, B. Foxen, S. Ganjam, R. Gasca, W. Giang, C. Gidney, D. Gilboa, M. Giustina, R. Gosula, A. G. Dau, D. Graumann, A. Greene, S. Habegger, M. C. Hamilton, M. Hansen, M. P. Harrigan, S. D. Harrington, S. Heslin, P. Heu, G. Hill, M. R. Hoffmann, H. Y. Huang, T. Huang, A. Huff, W. J. Huggins, S. V. Isakov, E. Jeffrey, Z. Jiang, C. Jones, S. Jordan, C. Joshi, P. Juhas, D. Kafri, H. Kang, K. Kechedzhi, T. Khaira, T. Khattar, M. Khezri, M. Kieferová, S. Kim, A. Kitaev, P. Klimov, A. N. Korotkov, F. Kostritsa, J. M. Kreikebaum, D. Landhuis, B. W. Langley, P. Laptev, K. M. Lau, L. L. Guevel, J. Ledford, J. Lee, K. W. Lee, Y. D. Lensky, B. J. Lester, W. Y. Li, A. T. Lill, W. Liu, W. P. Livingston, A. Locharla, D. Lundahl, A. Lunt, S. Madhuk, A. Maloney, S. Mandrà, L. S. Martin, O. Martin, S. Martin, C. Maxfield, J. R. McClean, M. McEwen, S. Meeks, K. C. Miao, A. Mieszala, S. Molina, S. Montazeri, A. Morvan, R. Movassagh, C. Neill, A. Nersisyan, M. Newman, A. Nguyen, M. Nguyen, C. H. Ni, M. Y. Niu, W. D. Oliver, K. Ottosson, A. Pizzuto, R. Potter, O. Pritchard, L. P. Pryadko, C. Quintana, M. J. Reagor, D. M. Rhodes, G. Roberts, C. Rocque, E. Rosenberg, N. C. Rubin, N. Saei, K. Sankaragomathi, K. J. Satzinger, H. F. Schurkus, C. Schuster, M. J. Shearn, A. Shorter, N. Shutty, V. Shvarts, V. Sivak, J. Skrzynny, S. Small, W. C. Smith, S. Springer, G. Sterling, J. Suchard, M. Szalay, A. Szein, D. Thor, A. Torres, M. M. Torunbalci, A. Vaishnav, S. Vdovichev, B. Villalonga, C. V. Heidweiller, S. Waltman, S. X. Wang, T. White, K. Wong, B. W. K. Woo, C. Xing, Z. J. Yao, P. Yeh, B. Ying, J. Yoo, N. Yosri, G. Young, A. Zalcman, N. Zhu, N. Zobrist, H. Neven, R. Babbush, S. Boixo, J. Hilton, E. Lucero, A. Megrant, J. Kelly, Y. Chen, V. Smelyanskiy, G. Vidal, P. Roushan, A. M. Läuchli, D. A. Abanin, and X. Mi, *Nature* **638**, 79 (2025).
- [19] T. I. Andersen, N. Astrakhantsev, A. H. Karamlou, J. Berndtsson, J. Motruk, A. Szasz, J. A. Gross, A. Schuckert, T. Westerhout, Y. Zhang, E. Forati, D. Rossi, B. Kobrin, A. D. Paolo, A. R. Klots, I. Drozdov, V. Kurilovich, A. Petukhov, L. B. Ioffe, A. Elben, A. Rath, V. Vitale, B. Vermersch, R. Acharya, L. A. Beni, K. Anderson, M. Ansmann, F. Arute, K. Arya, A. Asfaw, J. Atalaya, B. Ballard, J. C. Bardin, A. Bengtsson, A. Bilmes, G. Bortoli, A. Bourassa, J. Bovaird, L. Brill, M. Broughton, D. A. Browne, B. Buchea, B. B. Buckley, D. A. Buell, T. Burger, B. Burkett, N. Bushnell,

- A. Cabrera, J. Campero, H. S. Chang, Z. Chen, B. Chiaro, J. Claes, A. Y. Cleland, J. Cogan, R. Collins, P. Conner, W. Courtney, A. L. Crook, S. Das, D. M. Debroy, L. D. Lorenzo, A. D. T. Barba, S. Demura, P. Donohoe, A. Dunsworth, C. Earle, A. Eickbusch, A. M. Elbag, M. Elzouka, C. Erickson, L. Faoro, R. Fatemi, V. S. Ferreira, L. F. Burgos, A. G. Fowler, B. Foxen, S. Ganjam, R. Gasca, W. Giang, C. Gidney, D. Gilboa, M. Giustina, R. Gosula, A. G. Dau, D. Graumann, A. Greene, S. Habegger, M. C. Hamilton, M. Hansen, M. P. Harrigan, S. D. Harrington, S. Heslin, P. Heu, G. Hill, M. R. Hoffmann, H. Y. Huang, T. Huang, A. Huff, W. J. Huggins, S. V. Isakov, E. Jeffrey, Z. Jiang, C. Jones, S. Jordan, C. Joshi, P. Juhas, D. Kafri, H. Kang, K. Kechedzhi, T. Khairé, T. Khattar, M. Khezri, M. Kieferová, S. Kim, A. Kitaev, P. Klimov, A. N. Korotkov, F. Kostritsa, J. M. Kreikebaum, D. Landhuis, B. W. Langley, P. Laptev, K. M. Lau, L. L. Guevel, J. Ledford, J. Lee, K. W. Lee, Y. D. Lensky, B. J. Lester, W. Y. Li, A. T. Lill, W. Liu, W. P. Livingston, A. Locharla, D. Lundahl, A. Lunt, S. Madhuk, A. Maloney, S. Mandrà, L. S. Martin, O. Martin, S. Martin, C. Maxfield, J. R. McClean, M. McEwen, S. Meeks, K. C. Miao, A. Mieszala, S. Molina, S. Montazeri, A. Morvan, R. Movassagh, C. Neill, A. Nersisyan, M. Newman, A. Nguyen, M. Nguyen, C. H. Ni, M. Y. Niu, W. D. Oliver, K. Ottosson, A. Pizzuto, R. Potter, O. Pritchard, L. P. Pryadko, C. Quintana, M. J. Reagor, D. M. Rhodes, G. Roberts, C. Rocque, E. Rosenberg, N. C. Rubin, N. Saei, K. Sankaragomathi, K. J. Satzinger, H. F. Schurkus, C. Schuster, M. J. Shearn, A. Shorter, N. Shutty, V. Shvarts, V. Sivak, J. Skrzuzny, S. Small, W. C. Smith, S. Springer, G. Sterling, J. Suchard, M. Szalay, A. Sztein, D. Thor, A. Torres, M. M. Torunbalci, A. Vaishnav, S. Vdovichev, B. Villalonga, C. V. Heidweiller, S. Waltman, S. X. Wang, T. White, K. Wong, B. W. K. Woo, C. Xing, Z. J. Yao, P. Yeh, B. Ying, J. Yoo, N. Yosri, G. Young, A. Zalcman, N. Zhu, N. Zobrist, H. Neven, R. Babbush, S. Boixo, J. Hilton, E. Lucero, A. Megrant, J. Kelly, Y. Chen, V. Smelyanskiy, G. Vidal, P. Roushan, A. M. Läuchli, D. A. Abanin, and X. Mi, *Nature* **638**, 79 (2025).
- [20] T. Kohlert, S. Scherg, P. Sala, F. Pollmann, B. Hebbe Madhusudhana, I. Bloch, and M. Aidelsburger, *Phys. Rev. Lett.* **130**, 010201 (2023).
- [21] X. Liang, Z. Yue, Y.-X. Chao, Z.-X. Hua, Y. Lin, M. Khoon Tey, and L. You, *arXiv e-prints*, arXiv:2410.16174 (2024), arXiv:2410.16174 [quant-ph].
- [22] M. Xu, L. H. Kendrick, A. Kale, Y. Gang, C. Feng, S. Zhang, A. W. Young, M. Lebrat, and M. Greiner, *Nature* **642**, 909 (2025).
- [23] A. Mazurenko, C. S. Chiu, G. Ji, M. F. Parsons, M. Kanász-Nagy, R. Schmidt, F. Grusdt, E. Demler, D. Greif, and M. Greiner, *Nature* **545**, 462 (2017).
- [24] X. Wang, E. Khatami, F. Fei, J. Wyrick, P. Namboodiri, R. Kashid, A. F. Rigosi, G. Bryant, and R. Silver, *Nature Communications* **13**, 6824 (2022).
- [25] C. Hofrichter, L. Riegger, F. Scazza, M. Höfer, D. R. Fernandes, I. Bloch, and S. Fölling, *Phys. Rev. X* **6**, 021030 (2016).
- [26] H.-J. Shao, Y.-X. Wang, D.-Z. Zhu, Y.-S. Zhu, H.-N. Sun, S.-Y. Chen, C. Zhang, Z.-J. Fan, Y. Deng, X.-C. Yao, Y.-A. Chen, and J.-W. Pan, *Nature* **632**, 267 (2024).
- [27] C. Gross and I. Bloch, *Science* **357**, 995 (2017), <https://www.science.org/doi/pdf/10.1126/science.aal3837>.
- [28] P. Sompet, S. Hirthe, D. Bourgund, T. Chalopin, J. Bibo, J. Koepsell, P. Bojović, R. Verresen, F. Pollmann, G. Salomon, C. Gross, T. A. Hilker, and I. Bloch, *Nature* **606**, 484 (2022).
- [29] Z. Yue, Y.-F. Mao, X. Liang, Z.-X. Hua, P. Ge, Y.-X. Chao, K. Li, C. Jia, M. Khoon Tey, Y. Xu, and L. You, *arXiv e-prints*, arXiv:2505.06286 (2025), arXiv:2505.06286 [cond-mat.quant-gas].
- [30] Y. Lu, C. Wang, S. K. Kanungo, F. B. Dunning, and T. C. Killian, *Phys. Rev. A* **110**, 023318 (2024).
- [31] S. de Léséleuc, V. Lienhard, P. Scholl, D. Barredo, S. Weber, N. Lang, H. P. Büchler, T. Lahaye, and A. Browaeys, *Science* **365**, 775 (2019), <https://www.science.org/doi/pdf/10.1126/science.aav9105>.
- [32] D. González-Cuadra, M. Hamdan, T. V. Zache, B. Braverman, M. Kornjača, A. Lukin, S. H. Cantú, F. Liu, S.-T. Wang, A. Keesling, M. D. Lukin, P. Zoller, and A. Bylinskii, *Nature* **642**, 321 (2025).
- [33] J. Mildenerger, W. Mruczkiewicz, J. C. Halimeh, Z. Jiang, and P. Hauke, *Nature Physics* **21**, 312 (2025).
- [34] D. D'Alessandro, *Introduction to Quantum Control and Dynamics*, 2nd ed. (Chapman and Hall/CRC, 2021).
- [35] S. C. Benjamin, *Phys. Rev. A* **61**, 020301 (2000).
- [36] S. C. Benjamin, *Phys. Rev. Lett.* **88**, 017904 (2001).
- [37] S. Lloyd, *Quantum approximate optimization is computationally universal* (2018), arXiv:1812.11075 [quant-ph].
- [38] F. Cesa and H. Pichler, *Phys. Rev. Lett.* **131**, 170601 (2023).
- [39] F. Gkritis, D. Dux, J. Zhang, N. Jain, C. Gogolin, and P. M. Preiss, *PRX Quantum* **6**, 010318 (2025).
- [40] T. Chalopin, *Nature Reviews Physics* **3**, 605 (2021).
- [41] T. Chalopin, P. Bojović, D. Bourgund, S. Wang, T. Franz, I. Bloch, and T. Hilker, *Phys. Rev. Lett.* **134**, 053402 (2025).
- [42] Z. Manchester and S. Kuindersma, *Auton. Robots* **43**, 375–387 (2019).
- [43] A. J. Goldschmidt, J. L. DuBois, S. L. Brunton, and J. N. Kutz, *Quantum* **6**, 837 (2022).
- [44] A. Trowbridge, A. Bhardwaj, K. He, D. I. Schuster, and Z. Manchester, in *2023 IEEE International Conference on Quantum Computing and Engineering (QCE)*, Vol. 1 (IEEE, 2023) pp. 1278–1285.
- [45] N. Goldman and J. Dalibard, *Phys. Rev. X* **4**, 031027 (2014).
- [46] P. Bordia, H. Lüschen, U. Schneider, M. Knap, and I. Bloch, *Nature Physics* **13**, 460 (2017).
- [47] D. Bluvstein, A. Omran, H. Levine, A. Keesling, G. Semeghini, S. Ebadi, T. T. Wang, A. A. Michailidis, N. Maskara, W. W. Ho, S. Choi, M. Serbyn, M. Greiner, V. Vuletić, and M. D. Lukin, *Science* **371**, 1355 (2021), <https://www.science.org/doi/pdf/10.1126/science.abg2530>.
- [48] S. Geier, N. Thaicharoen, C. Hainaut, T. Franz, A. Salzinger, A. Tebben, D. Grimshandl, G. Zürn, and M. Weidemüller, *Science* **374**, 1149 (2021), <https://www.science.org/doi/pdf/10.1126/science.abd9547>.
- [49] N. Uğur Köyliüoğlu, N. Maskara, J. Feldmeier, and M. D. Lukin, *arXiv e-prints*, arXiv:2408.02741 (2024), arXiv:2408.02741 [quant-ph].

- [50] N. Khaneja, T. Reiss, C. Kehlet, T. Schulte-Herbrüggen, and S. J. Glaser, *Journal of Magnetic Resonance* **172**, 296 (2005).
- [51] R. Verresen, R. Moessner, and F. Pollmann, *Phys. Rev. B* **96**, 165124 (2017).
- [52] G. Semeghini, H. Levine, A. Keesling, S. Ebadi, T. T. Wang, D. Bluvstein, R. Verresen, H. Pichler, M. Kalinowski, R. Samajdar, A. Omran, S. Sachdev, A. Vishwanath, M. Greiner, V. Vuletić, and M. D. Lukin, *Science* **374**, 1242 (2021), <https://www.science.org/doi/pdf/10.1126/science.abi8794>.
- [53] D. Bluvstein, A. Omran, H. Levine, A. Keesling, G. Semeghini, S. Ebadi, T. T. Wang, A. A. Michailidis, N. Maskara, W. W. Ho, S. Choi, M. Serbyn, M. Greiner, V. Vuletić, and M. D. Lukin, *Science* **371**, 1355 (2021), <https://www.science.org/doi/pdf/10.1126/science.abg2530>.
- [54] D. Jaksch, J. I. Cirac, P. Zoller, S. L. Rolston, R. Côté, and M. D. Lukin, *Phys. Rev. Lett.* **85**, 2208 (2000).
- [55] H. Labuhn, D. Barredo, S. Ravets, S. de Léséleuc, T. Macrì, T. Lahaye, and A. Browaeys, *Nature* **534**, 667 (2016).
- [56] S. Lloyd, *Science* **273**, 1073 (1996), <https://www.science.org/doi/pdf/10.1126/science.273.5278.1073>.
- [57] S. Lloyd, *Phys. Rev. Lett.* **75**, 346 (1995).
- [58] M. J. Bremner, C. M. Dawson, J. L. Dodd, A. Gilchrist, A. W. Harrow, D. Mortimer, M. A. Nielsen, and T. J. Osborne, *Phys. Rev. Lett.* **89**, 247902 (2002).
- [59] M. A. Nielsen and I. L. Chuang, *Quantum Computation and Quantum Information: 10th Anniversary Edition* (Cambridge University Press, 2010).
- [60] M. Ragone, B. N. Bakalov, F. Sauvage, A. F. Kemper, C. Ortiz Marrero, M. Larocca, and M. Cerezo, *Nature Communications* **15**, 7172 (2024).
- [61] R. Wiersema, E. Kökcü, A. F. Kemper, and B. N. Bakalov, *npj Quantum Information* **10**, 110 (2024).
- [62] J. Allcock, M. Santha, P. Yuan, and S. Zhang, *arXiv e-prints*, arXiv:2407.12587 (2024), arXiv:2407.12587 [quant-ph].
- [63] D. D'Alessandro, *arXiv e-prints*, arXiv:0803.1193 (2008), arXiv:0803.1193 [quant-ph].
- [64] R. A. Bravo, J. G. Ponce, H.-Y. Hu, and S. F. Yelin, *APL Quantum* **1**, 046121 (2024), https://pubs.aip.org/aip/apq/article-pdf/doi/10.1063/5.0235279/20289864/046121_1.5.0235279.pdf.
- [65] A. Barenco, C. H. Bennett, R. Cleve, D. P. DiVincenzo, N. Margolus, P. Shor, T. Sleator, J. A. Smolin, and H. Weinfurter, *Phys. Rev. A* **52**, 3457 (1995).
- [66] S. Anand, C. E. Bradley, R. White, V. Ramesh, K. Singh, and H. Bernien, *Nature Physics* **20**, 1744 (2024).
- [67] M. Oszmaniec and Z. Zimborás, *Physical Review Letters* **119**, 10.1103/physrevlett.119.220502 (2017).
- [68] D. K. Mark, H.-Y. Hu, J. Kwan, C. Kokail, S. Choi, and S. F. Yelin, *arXiv e-prints*, arXiv:2412.13186 (2024), arXiv:2412.13186 [cond-mat.quant-gas].
- [69] E. Dagotto, *Rev. Mod. Phys.* **66**, 763 (1994).
- [70] S. R. White and D. J. Scalapino, *Phys. Rev. B* **61**, 6320 (2000).
- [71] E. Pavarini, I. Dasgupta, T. Saha-Dasgupta, O. Jepsen, and O. K. Andersen, *Phys. Rev. Lett.* **87**, 047003 (2001).
- [72] T. Maier, M. Jarrell, T. Pruschke, and M. H. Hettler, *Rev. Mod. Phys.* **77**, 1027 (2005).
- [73] X.-G. Wen, *Rev. Mod. Phys.* **89**, 041004 (2017).
- [74] X.-L. Qi and S.-C. Zhang, *Rev. Mod. Phys.* **83**, 1057 (2011).
- [75] Q.-R. Wang and Z.-C. Gu, *Phys. Rev. X* **8**, 011055 (2018).
- [76] M. Cheng, Z. Bi, Y.-Z. You, and Z.-C. Gu, *Phys. Rev. B* **97**, 205109 (2018).
- [77] C. M. Duque, H.-Y. Hu, Y.-Z. You, V. Khemani, R. Verresen, and R. Vasseur, *Phys. Rev. B* **103**, L100207 (2021).
- [78] G. Giudici, M. D. Lukin, and H. Pichler, *Phys. Rev. Lett.* **129**, 090401 (2022).
- [79] Y. Lu, C. Wang, S. K. Kanungo, F. B. Dunning, and T. C. Killian, *Phys. Rev. A* **110**, 023318 (2024).
- [80] Y.-J. Liu, K. Shtengel, and F. Pollmann, *Phys. Rev. Res.* **6**, 043256 (2024).
- [81] X. Zhang, W. Jiang, J. Deng, K. Wang, J. Chen, P. Zhang, W. Ren, H. Dong, S. Xu, Y. Gao, F. Jin, X. Zhu, Q. Guo, H. Li, C. Song, A. V. Gorshkov, T. Iadecola, F. Liu, Z.-X. Gong, Z. Wang, D.-L. Deng, and H. Wang, *Nature* **607**, 468 (2022).
- [82] P. T. Dumitrescu, J. G. Bohnet, J. P. Gaebler, A. Hankin, D. Hayes, A. Kumar, B. Neyenhuis, R. Vasseur, and A. C. Potter, *Nature* **607**, 463 (2022).
- [83] M. Iqbal, N. Tantivasadakarn, R. Verresen, S. L. Campbell, J. M. Dreiling, C. Figgatt, J. P. Gaebler, J. Johansen, M. Mills, S. A. Moses, J. M. Pino, A. Ransford, M. Rowe, P. Siegfried, R. P. Stutz, M. Foss-Feig, A. Vishwanath, and H. Dreyer, *Nature* **626**, 505 (2024).
- [84] T. I. Andersen, Y. D. Lensky, K. Kechedzhi, I. K. Drozdov, A. Bengtsson, S. Hong, A. Morvan, X. Mi, A. Opremcak, R. Acharya, R. Allen, M. Ansmann, F. Arute, K. Arya, A. Asfaw, J. Atalaya, R. Babbush, D. Bacon, J. C. Bardin, G. Bortoli, A. Bourassa, J. Bovaird, L. Brill, M. Broughton, B. B. Buckley, D. A. Buell, T. Burger, B. Burkett, N. Bushnell, Z. Chen, B. Chiaro, D. Chik, C. Chou, J. Cogan, R. Collins, P. Conner, W. Courtney, A. L. Crook, B. Curtin, D. M. Debroy, A. Del Toro Barba, S. Demura, A. Dunsworth, D. Eppens, C. Erickson, L. Faoro, E. Farhi, R. Fatemi, V. S. Ferreira, L. F. Burgos, E. Forati, A. G. Fowler, B. Foxen, W. Giang, C. Gidney, D. Gilboa, M. Giustina, R. Gosula, A. G. Dau, J. A. Gross, S. Habegger, M. C. Hamilton, M. Hansen, M. P. Harrigan, S. D. Harrington, P. Heu, J. Hilton, M. R. Hoffmann, T. Huang, A. Huff, W. J. Huggins, L. B. Ioffe, S. V. Isakov, J. Iveland, E. Jeffrey, Z. Jiang, C. Jones, P. Juhas, D. Kafri, T. Khatyar, M. Khezri, M. Kieferová, S. Kim, A. Kitaev, P. V. Klimov, A. R. Klots, A. N. Korotkov, F. Kostritsa, J. M. Kreikebaum, D. Landhuis, P. Laptev, K. M. Lau, L. Laws, J. Lee, K. W. Lee, B. J. Lester, A. T. Lill, W. Liu, A. Locharla, E. Lucero, F. D. Malone, O. Martin, J. R. McClean, T. McCourt, M. McEwen, K. C. Miao, A. Mieszala, M. Mohseni, S. Montazeri, E. Mount, R. Movassagh, W. Mruzekiewicz, O. Naaman, M. Neeley, C. Neill, A. Nersisyan, M. Newman, J. H. Ng, A. Nguyen, M. Nguyen, M. Y. Niu, T. E. O'Brien, S. Omonije, A. Petukhov, R. Potter, L. P. Pryadko, C. Quintana, C. Rocque, N. C. Rubin, N. Saei, D. Sank, K. Sankaragomathi, K. J. Satzinger,

- H. F. Schurkus, C. Schuster, M. J. Shearn, A. Shorter, N. Shutty, V. Shvarts, J. Skruzny, W. C. Smith, R. Somma, G. Sterling, D. Strain, M. Szalay, A. Torres, G. Vidal, B. Villalonga, C. V. Heidweiller, T. White, B. W. K. Woo, C. Xing, Z. J. Yao, P. Yeh, J. Yoo, G. Young, A. Zalcman, Y. Zhang, N. Zhu, N. Zobrist, H. Neven, S. Boixo, A. Megrant, J. Kelly, Y. Chen, V. Smelyanskiy, E. A. Kim, I. Aleiner, P. Roushan, G. Q. AI, and Collaborators, *Nature* **618**, 264 (2023).
- [85] L. Chen, Y. Ren, R. Fan, and A. Jaffe, *npj Quantum Information* **11**, 112 (2025).
- [86] E. Urban, T. A. Johnson, T. Henage, L. Isenhower, D. D. Yavuz, T. G. Walker, and M. Saffman, *Nature Physics* **5**, 110 (2009).
- [87] R. Trivedi, A. Franco Rubio, and J. I. Cirac, *Nature Communications* **15**, 6507 (2024).
- [88] A. J. Daley, I. Bloch, C. Kokail, S. Flannigan, N. Pearson, M. Troyer, and P. Zoller, *Nature* **607**, 667 (2022).
- [89] A. Kitaev, in *Advances in Theoretical Physics: Landau Memorial Conference*, American Institute of Physics Conference Series, Vol. 1134, edited by V. Lebedev and M. Feigel'Man (AIP, 2009) pp. 22–30, [arXiv:0901.2686](https://arxiv.org/abs/0901.2686) [cond-mat.mes-hall].
- [90] J. Wurtz, A. Bylinskii, B. Braverman, J. Amato-Grill, S. H. Cantu, F. Huber, A. Lukin, F. Liu, P. Weinberg, J. Long, S.-T. Wang, N. Gemelke, and A. Keesling, *arXiv e-prints*, [arXiv:2306.11727](https://arxiv.org/abs/2306.11727) (2023), [arXiv:2306.11727](https://arxiv.org/abs/2306.11727) [quant-ph].
- [91] N. Maskara, S. Ostermann, J. Shee, M. Kalinowski, A. McClain Gomez, R. Araiza Bravo, D. S. Wang, A. I. Krylov, N. Y. Yao, M. Head-Gordon, M. D. Lukin, and S. F. Yelin, *Nature Physics* **21**, 289 (2025).
- [92] S. J. Evered, M. Kalinowski, A. A. Geim, T. Manovitz, D. Bluvstein, S. H. Li, N. Maskara, H. Zhou, S. Ebadi, M. Xu, J. Campo, M. Cain, S. Ostermann, S. F. Yelin, S. Sachdev, M. Greiner, V. Vuletić, and M. D. Lukin, *arXiv e-prints*, [arXiv:2501.18554](https://arxiv.org/abs/2501.18554) (2025), [arXiv:2501.18554](https://arxiv.org/abs/2501.18554) [quant-ph].
- [93] J. T. Betts, *Journal of Guidance, Control, and Dynamics* **21**, 193 (1998), <https://doi.org/10.2514/2.4231>.
- [94] M. Kelly, *SIAM Review* **59**, 849 (2017), <https://doi.org/10.1137/16M1062569>.
- [95] J. T. Betts, *Practical Methods for Optimal Control Using Nonlinear Programming, Third Edition* (Society for Industrial and Applied Mathematics, Philadelphia, PA, 2020) <https://epubs.siam.org/doi/pdf/10.1137/1.9781611976199>.
- [96] Here, we emphasize that unitary fidelity may be an overly stringent metric, as analog simulations typically focus on local observables and signals, which are often more robust and perform better than global measures like unitary fidelity [87].
- [97] J. Z. Lu, L. Jiao, K. Wolinski, M. Kornjača, H.-Y. Hu, S. Cantu, F. Liu, S. F. Yelin, and S.-T. Wang, *Quantum Science and Technology* **10**, 015038 (2025), [arXiv:2401.02940](https://arxiv.org/abs/2401.02940) [quant-ph].
- [98] A. Michel, S. Grijalva, L. Henriot, C. Domain, and A. Browaeys, *Phys. Rev. A* **107**, 042602 (2023).
- [99] We include a multiplicative shift term $k\Omega(t)$ in the model for $\Omega(t)$ because calibration experiments, including our own and those described in Ref. [119], indicate that the control error varies with the input values.
- [100] A. Gu, L. Cincio, and P. J. Coles, *Nature Communications* **15**, 312 (2024).
- [101] D. Hangleiter, I. Roth, J. Fuksa, J. Eisert, and P. Roushan, *Nature Communications* **15**, 9595 (2024).
- [102] H.-Y. Hu, A. Gu, S. Majumder, H. Ren, Y. Zhang, D. S. Wang, Y.-Z. You, Z. Mineev, S. F. Yelin, and A. Seif, *Nature Communications* **16**, 2943 (2025).
- [103] H.-Y. Hu, M. Ma, W. Gong, Q. Ye, Y. Tong, S. T. Flammia, and S. F. Yelin, *arXiv e-prints*, [arXiv:2502.11900](https://arxiv.org/abs/2502.11900) (2025), [arXiv:2502.11900](https://arxiv.org/abs/2502.11900) [quant-ph].
- [104] H.-Y. Huang, R. Kueng, and J. Preskill, *Nature Physics* **16**, 1050 (2020).
- [105] A. Elben, S. T. Flammia, H.-Y. Huang, R. Kueng, J. Preskill, B. Vermersch, and P. Zoller, *Nature Reviews Physics* **5**, 9 (2023).
- [106] M. S. Rudolph, T. Jones, Y. Teng, A. Angrisani, and Z. Holmes, *arXiv e-prints*, [arXiv:2505.21606](https://arxiv.org/abs/2505.21606) (2025), [arXiv:2505.21606](https://arxiv.org/abs/2505.21606) [quant-ph].
- [107] V. Martinez, A. Angrisani, E. Pankovets, O. Fawzi, and D. Stilck França, *Phys. Rev. Lett.* **134**, 250602 (2025).
- [108] Y. Shao, F. Wei, S. Cheng, and Z. Liu, *Phys. Rev. Lett.* **133**, 120603 (2024).
- [109] S. Patra, S. S. Jahromi, S. Singh, and R. Orús, *Phys. Rev. Res.* **6**, 013326 (2024).
- [110] J. Tindall, M. Fishman, E. M. Stoudenmire, and D. Sels, *PRX Quantum* **5**, 010308 (2024).
- [111] J. Tindall and M. Fishman, *SciPost Phys.* **15**, 222 (2023).
- [112] M. S. Rudolph and J. Tindall, *arXiv e-prints*, [arXiv:2507.11424](https://arxiv.org/abs/2507.11424) (2025), [arXiv:2507.11424](https://arxiv.org/abs/2507.11424) [quant-ph].
- [113] V. V. Sivak, A. Eickbusch, H. Liu, B. Royer, I. Tsioutsios, and M. H. Devoret, *Phys. Rev. X* **12**, 011059 (2022).
- [114] H.-Y. Huang, Y. Liu, M. Broughton, I. Kim, A. Anshu, Z. Landau, and J. R. McClean, in *Proceedings of the 56th Annual ACM Symposium on Theory of Computing*, STOC 2024 (Association for Computing Machinery, New York, NY, USA, 2024) p. 1343–1351.
- [115] Y. Cao, S. Liu, H. Deng, Z. Xia, X. Wu, and Y.-X. Wang, *arXiv e-prints*, [arXiv:2412.07764](https://arxiv.org/abs/2412.07764) (2024), [arXiv:2412.07764](https://arxiv.org/abs/2412.07764) [quant-ph].
- [116] M. Goll and R. H. Jonsson, *arXiv e-prints*, [arXiv:2504.15175](https://arxiv.org/abs/2504.15175) (2025), [arXiv:2504.15175](https://arxiv.org/abs/2504.15175) [quant-ph].
- [117] M. Wiedmann and D. Burgarth, *arXiv e-prints*, [arXiv:2506.10069](https://arxiv.org/abs/2506.10069) (2025), [arXiv:2506.10069](https://arxiv.org/abs/2506.10069) [quant-ph].
- [118] M. A. Nielsen, *Quantum Info. Comput.* **6**, 213–262 (2006).
- [119] C. B. Dag, H. Ma, P. Myles Eugenio, F. Fang, and S. F. Yelin, *arXiv e-prints*, [arXiv:2411.13643](https://arxiv.org/abs/2411.13643) (2024), [arXiv:2411.13643](https://arxiv.org/abs/2411.13643) [quant-ph].
- [120] B. Hall, *Lie Groups, Lie Algebras, and Representations: An Elementary Introduction*, Graduate Texts in Mathematics (Springer, 2003).
- [121] W. Rossmann, *Lie Groups: An Introduction Through Linear Groups*, Oxford Mathematics (Oxford University Press, 2006).
- [122] M. Suzuki, *Communications in Mathematical Physics* **51**, 183 (1976).
- [123] M. Suzuki, *Communications in Mathematical Physics* **57**, 193 (1977).
- [124] A. Sagle and R. Walde, *Introduction to Lie Groups and Lie Algebra*, 51 (Academic Press, 1986).

- [125] S. B. Bravyi and A. Y. Kitaev, *Annals of Physics* **298**, 210–226 (2002).
- [126] B. M. Terhal and D. P. DiVincenzo, *Physical Review A* **65**, 10.1103/physreva.65.032325 (2002).
- [127] D. P. DiVincenzo and B. M. Terhal, *Foundations of Physics* **35**, 1967–1984 (2005).
- [128] T. Chalopin, P. Bojović, D. Bourgund, S. Wang, T. Franz, I. Bloch, and T. Hilker, *Phys. Rev. Lett.* **134**, 053402 (2025).
- [129] C. J. Turner, A. A. Michailidis, D. A. Abanin, M. Serbyn, and Z. Papić, *Physical Review B* **98**, 10.1103/physrevb.98.155134 (2018).
- [130] N. Khaneja, T. Reiss, C. Kehlet, T. Schulte-Herbrüggen, and S. J. Glaser, *Journal of magnetic resonance* **172**, 296 (2005).
- [131] H. A. Rabitz, M. M. Hsieh, and C. M. Rosenthal, *Science* **303**, 1998 (2004).
- [132] A. G. R. Day, M. Bukov, P. Weinberg, P. Mehta, and D. Sels, *Phys. Rev. Lett.* **122**, 020601 (2019).
- [133] A. Wächter and L. T. Biegler, *Mathematical programming* **106**, 25 (2006).
- [134] B. Bhattacharyya, F. An, D. Kozbiel, A. J. Goldschmidt, and F. T. Chong, in *2024 IEEE International Conference on Quantum Computing and Engineering (QCE)*, Vol. 01 (2024) pp. 1336–1346.
- [135] A. J. Goldschmidt, E. Peláez Cisneros, R. Sitler, K. Olsson, K. N. Smith, and G. Quiroz, in preparation.
- [136] Harmoniqs, Piccolo.jl: Fine tuned quantum optimal control, <https://github.com/harmoniqs/Piccolo.jl> (2025), see <https://www.harmoniqs.co> for more information.
- [137] F. Sauvage and F. Mintert, *Physical Review Letters* **129**, 050507 (2022).
- [138] J. D. Chadwick and F. T. Chong, in *2023 IEEE International Conference on Quantum Computing and Engineering (QCE)*, Vol. 1 (IEEE, 2023) pp. 1286–1294.

Supplementary Material

Appendix A: Notations and Preliminaries

In this work, we use X, Y, Z to denote the Pauli matrices. The N -fold tensor products of single-qubit Pauli matrices along with the identity matrix are represented by \mathbb{P}_N :

$$\mathbb{P}_N := \left\{ \bigotimes_{i=1}^N P_i : P_i = I, X, Y, Z \right\}. \quad (\text{A1})$$

The subscript i indicates that the operator is applied to the i -th qubit. We typically omit the identity matrix when writing a multi-qubit Pauli operator, such as $I_1 Z_2 Z_3 I_4 \rightarrow Z_2 Z_3$.

We use c_i^\dagger and c_i (b_i^\dagger and b_i) to represent the fermionic (bosonic) creation and annihilation operators at site i , respectively. They satisfy the following canonical commutation relations:

$$\{c_i, c_i^\dagger\} = \delta_{ij}, \quad \{c_i^\dagger, c_j^\dagger\} = \{c_i, c_j\} = 0, \quad [b_i, b_i^\dagger] = \delta_{ij}, \quad [b_i^\dagger, b_j^\dagger] = [b_i, b_j] = 0, \quad (\text{A2})$$

where $\{A, B\} = AB + BA$ and $[A, B] = AB - BA$ are the anticommutator and commutator, respectively. The following commutation relations are frequently used in our proof of universality:

$$\begin{aligned} [AB, CD] &= A[B, C]D + AC[B, D] + [A, C]DB + C[A, D]B, \\ [AB, CD] &= A\{B, C\}D - AC\{B, D\} + \{A, C\}DB - C\{A, D\}B. \end{aligned} \quad (\text{A3})$$

In the quantum control literature, when studying the expressivity of a given set of control pulses, people explore its attainable effective evolution based on the Baker-Campbell-Hausdorff (BCH), which is defined as follows [120, 121]:

Definition 1 (The Baker-Campbell-Hausdorff formula). *Given two elements A, B in a Lie algebra, the Baker-Campbell-Hausdorff (BCH) formula gives the element C which solves the following equation:*

$$e^A e^B = e^C,$$

in case this equation has a solution. To the first four orders of the commutator, the explicit formula of Z is:

$$C(A, B) = A + B + \frac{1}{2}[A, B] + \frac{1}{12}([A, [A, B]] + [B, [B, A]]) - \frac{1}{24}[B, [A, [A, B]]] + \dots, \quad (\text{A4})$$

where \dots represents the higher order terms.

When specific to quantum unitary evolution, A, B and C take the form of anti-Hermitian operators iH for some Hermitian H . This ensures both sides of Equation (A4) are consistent. Given a quantum control system with control Hamiltonians H_1, H_2, \dots, H_l , we can define a generating set $\mathcal{G} = \{iH_1, iH_2, \dots, iH_l\}$. Then, the physically obtainable evolution is determined by the *Dynamical Lie Algebra* (DLA) generated by \mathcal{G} , which is defined by:

Definition 2 (Dynamical Lie Algebra). *Given a control system with generators $\mathcal{G} = \{iH_1, iH_2, \dots, iH_l\}$, the Dynamical Lie Algebra (DLA) \mathfrak{g} is the subalgebra of $\mathfrak{su}(d)$ spanned by the repeated nested commutators of the elements in \mathcal{G} , i.e.*

$$\mathfrak{g} = \text{span}_{\mathbb{R}}\langle iH_1, iH_2, \dots, iH_l \rangle_{\text{Lie}} \subseteq \mathfrak{su}(d),$$

where $\text{span}_{\mathbb{R}}\langle iH_1, iH_2, \dots, iH_l \rangle_{\text{Lie}}$ denotes the Lie closure under nested commutators, and d is the dimension of the Hilbert space.

In Definition 2, the k -th order nested commutator of \mathcal{G} is defined by $[G_1, [G_2, \dots, [G_{k-1}, G_k]]]$ for $G_1, G_2, \dots, G_k \in \mathcal{G}$. The DLA \mathfrak{g} contains all linear combinations (with real coefficients for anti-Hermiticity) of those nested commutators with arbitrary orders. For a specific task like quantum computation or quantum simulation, there is a largest subalgebra of $\mathfrak{su}(d)$ one can attain. If \mathfrak{g} equals this subalgebra, it is termed *universal*, as detailed in Appendices B and C.

To understand why \mathfrak{g} is the attainable evolution given the control \mathcal{G} , we first notice that there are two basic operations generating the algebra \mathfrak{g} : (1) linear combination and (2) Lie bracket of arbitrary two elements in \mathfrak{g} . Starting with an initial algebra $\mathfrak{g}_0 \equiv \mathcal{G}$, we can construct an enlarged algebra \mathfrak{g}_1 by adding linearly independent

operators obtained from linear combining and commuting any two elements in \mathfrak{g}_0 . Then we can repeat the process for \mathfrak{g}_1 to obtain \mathfrak{g}_2 , until no non-trivial new elements can be found. This gives the final closed algebra \mathfrak{g} . From the above analysis, to conclude that \mathfrak{g} is attainable by the control in \mathcal{G} , it is sufficient to prove that the evolutions under (1) and (2) are realizable by the physical system. This is done in the proofs of Lemmas 2 and 3 below. The alternative proofs using the Trotter-Suzuki formula [122, 123] can be found in standard textbooks on Lie algebras, such as Theorem 5.16 in [124].

Lemma 2. *Consider a repertoire of unitary dynamics on a finite-dimensional Hilbert space. If the generated dynamics of a pair of Hermitian operators (Hamiltonians) H_1 and H_2 are in the repertoire, then every operation or unitary dynamics generated by $\alpha H_1 + \beta H_2$ is also in the repertoire.*

Proof. For any bounded A and B , the Lie-product (Trotter) formula converges in norm. Let $\Sigma_2^A = \sum_{n=2}^{\infty} A^n/n!$. By the fundamental theorem of calculus,

$$\Sigma_2^A = A^2 \int_0^1 ds \int_0^s dt e^{tA}, \quad \text{so} \quad \|\Sigma_2^A\| \leq \frac{\|A\|^2}{2} e^{\|A\|}. \quad \text{Thus} \quad \|\Sigma_2^{A/n}\| \leq \frac{\|A\|}{2n^2} e^{\|A\|/n}. \quad (\text{A5})$$

Then

$$\left\| e^{(A+B)/n} - e^{A/n} e^{B/n} \right\| \leq \left\| \Sigma_2^{(A+B)/n} - \Sigma_2^{A/n} \left(I + \frac{B}{n} \right) - \left(I + \frac{A}{n} \right) \Sigma_2^{B/n} - \Sigma_2^{A/n} \Sigma_2^{B/n} - \frac{AB}{n^2} \right\| \leq \frac{5}{n^2} e^{(\|A\| + \|B\|)/n}.$$

Thus we can expand the approximation to the formula into n terms, and have the bound

$$\left\| e^{A+B} - \left(e^{A/n} e^{B/n} \right)^n \right\| = \left\| \sum_{j=0}^{n-1} e^{j(A+B)/n} \left(e^{(A+B)/n} - e^{A/n} e^{B/n} \right) \left(e^{A/n} e^{B/n} \right)^{n-j-1} \right\| \leq \frac{5}{n} e^{\|A\| + \|B\|}. \quad (\text{A6})$$

By taking $A = i\alpha H_1$ and $B = i\beta H_2$ for some real numbers α and β , in the asymptotic limit $n \rightarrow \infty$:

$$e^{i(\alpha H_1 + \beta H_2)} = \lim_{n \rightarrow \infty} \left(e^{i\alpha H_1/n} e^{i\beta H_2/n} \right)^n,$$

so the evolution under $\alpha H_1 + \beta H_2$ is simulable given the control of H_1 and H_2 . \square

Lemma 3. *Consider a repertoire of unitary dynamics on a finite-dimensional Hilbert space. If the generated unitary dynamics of a pair of Hermitian operators (Hamiltonians) H_1 and H_2 are in the repertoire, then every operation or unitary dynamics generated by the commutator $i[H_1, H_2]$ is also in the repertoire. We prove a modified Trotter formula for bounded, self-adjoint generators H_j .*

$$e^{-[H_1, H_2]} = \lim_{n \rightarrow \infty} \left(e^{iH_1/\sqrt{n}} e^{iH_2/\sqrt{n}} e^{-iH_1/\sqrt{n}} e^{-iH_2/\sqrt{n}} \right)^n. \quad (\text{A7})$$

This may be elsewhere in the literature, we have also found it in [124], remark 1g following Theorem 5.16.

Proof. We consider bounded and skew-Hermitian operators A and B . We have the following integral formula:

$$\begin{aligned} e^{A/\sqrt{n}} e^{B/\sqrt{n}} e^{-A/\sqrt{n}} e^{-B/\sqrt{n}} - I &= e^{sA/\sqrt{n}} e^{B/\sqrt{n}} e^{-sA/\sqrt{n}} e^{-B/\sqrt{n}} \Big|_{s=0}^{s=1} \\ &= \frac{1}{\sqrt{n}} \int_0^1 ds e^{sA/\sqrt{n}} \left(A e^{B/\sqrt{n}} e^{-sA/\sqrt{n}} - e^{B/\sqrt{n}} A e^{-sA/\sqrt{n}} \right) e^{-B/\sqrt{n}} \\ &= \frac{1}{\sqrt{n}} \int_0^1 ds e^{sA/\sqrt{n}} \left[A, e^{B/\sqrt{n}} \right] e^{-sA/\sqrt{n}} e^{-B/\sqrt{n}}, \end{aligned} \quad (\text{A8})$$

where one can verify the second equality by taking a derivative of s on the left-hand side of the equation. Using the following identity:

$$e^{sA/\sqrt{n}} = I + \left(e^{sA/\sqrt{n}} - I \right) = I + \frac{A}{\sqrt{n}} \int_0^s dt e^{tA/\sqrt{n}}, \quad (\text{A9})$$

the Equation (A8) becomes:

$$\begin{aligned}
& \frac{1}{n} \int_0^1 ds \int_0^1 dt e^{sA/\sqrt{n}} \left[A, B e^{tB/\sqrt{n}} \right] e^{-sA/\sqrt{n}} e^{-B/\sqrt{n}} \\
&= \frac{1}{n} \int_0^1 ds \int_0^1 dt e^{sA/\sqrt{n}} \left([A, B] e^{tB/\sqrt{n}} + B \left[A, e^{tB/\sqrt{n}} \right] \right) e^{-sA/\sqrt{n}} e^{-B/\sqrt{n}} \\
&= \frac{[A, B]}{n} + R,
\end{aligned} \tag{A10}$$

where this defines R as the remainder. We now use the assumption that A and B are skew-Hermitian, so for real α, β, γ both $e^{\alpha A}$ and $e^{\beta B}$ are unitary, as is $e^{\gamma[A, B]}$. Note that in the last equality, we have used the integral identity in Equation (A9) to expand each exponential. Using

$$\left\| \left(e^{sA/\sqrt{n}} - I \right) \right\| \leq \frac{\|A\|}{\sqrt{n}}, \tag{A11}$$

and noticing that the remainder R contains at least one and at most four such terms of order $n^{-1/2}$, we have:

$$\|R\| \leq 2^6 (\|A\| + \|B\| + 1)^4 \frac{1}{n^{3/2}} = \frac{M}{n^{3/2}}, \tag{A12}$$

where M is a constant independent of n . Thus, the constant term and the linear term in the expansion of the exponential $e^{[A, B]/n}$ cancel with the corresponding terms in $e^{A/\sqrt{n}} e^{B/\sqrt{n}} e^{-A/\sqrt{n}} e^{-B/\sqrt{n}}$, which gives:

$$\left\| e^{[A, B]/n} - e^{A/\sqrt{n}} e^{B/\sqrt{n}} e^{-A/\sqrt{n}} e^{-B/\sqrt{n}} \right\| = \|R\| \leq \frac{M}{n^{3/2}}. \tag{A13}$$

By a similar expansion as in Equation (A6), we obtain:

$$\begin{aligned}
& \left\| e^{[A, B]} - \left(e^{A/\sqrt{n}} e^{B/\sqrt{n}} e^{-A/\sqrt{n}} e^{-B/\sqrt{n}} \right)^n \right\| \\
&= \left\| \sum_{j=0}^{n-1} e^{j[A, B]/n} \left(e^{[A, B]/n} - e^{A/\sqrt{n}} e^{B/\sqrt{n}} e^{-A/\sqrt{n}} e^{-B/\sqrt{n}} \right) \left(e^{A/\sqrt{n}} e^{B/\sqrt{n}} e^{-A/\sqrt{n}} e^{-B/\sqrt{n}} \right)^{n-j-1} \right\| \leq \frac{M}{\sqrt{n}}.
\end{aligned} \tag{A14}$$

Thus, by taking $A = iH_1$, $B = iH_2$, in the asymptotic limit $n \rightarrow \infty$:

$$e^{-[H_1, H_2]} = \lim_{n \rightarrow \infty} \left(e^{iH_1/\sqrt{n}} e^{iH_2/\sqrt{n}} e^{-iH_1/\sqrt{n}} e^{-iH_2/\sqrt{n}} \right)^n,$$

which completes the proof. \square

By Lemmas 2 and 3, we can understand the expressivity of a generating set \mathcal{G} by investigating its DLA \mathfrak{g} .

Appendix B: Universality of analog quantum computation

Here we detail the proof of Theorem 1, which establishes the sufficient and necessary condition for one-dimensional universal quantum computation under global control. Notably, in the qubit system, realizing universal quantum computation requires that the DLA \mathfrak{g} equals the whole algebra $\mathfrak{su}(2^N)$. Here, we rewrite the theorem in a formalized way for later convenience.

Theorem 1 (Minimal requirement for universal quantum computation on a qubit chain). *Consider a chain of qubits with homogeneous nearest neighbor Ising interactions $H_{ZZ} = \sum_j Z_j Z_{j+1}$. Suppose the system is equipped with tunable global X and Z fields, given by $H_X = \sum_j X_j$, $H_Z = \sum_j Z_j$. Then, suppose there are controllable X -fields globally applied to distinct subsets of lattice sites $\alpha = A, B, C, \dots$ with the Hamiltonian $H_{X, \alpha} = \sum_{j \in \alpha} X_j$. This system realizes universal quantum computation, i.e., $\mathfrak{g} = \text{span}_{\mathbb{R}}(iH_X, iH_Z, iH_{ZZ}, \cup_{\alpha} iH_{X, \alpha})_{\text{Lie}} = \mathfrak{su}(2^N)$, if and only if the combined pattern α breaks the lattice reflection symmetry.*

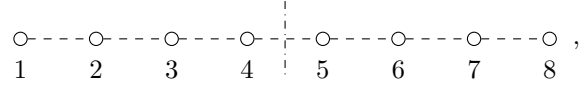
Remark 1. Compared to the original Theorem 1, here, we focus on the Ising-type nearest-neighbor interaction H_{ZZ} because its specific form is irrelevant. This is apparent later in the proof of Lemma 5. More specifically, as illustrated in Equation (B6), commuting H_X, H_Z with H_{ZZ} can generate arbitrary reflection-symmetric, uniform, nearest-neighbor interactions. Thus, all those interactions are included in the generating set, and it suffices to choose any one of them.

Moreover, we choose the symmetry-breaking field H_{break} in the original Theorem 1 to be the controllable X -fields $H_{X,\alpha}$ for convenience. This is reasonable because the specific form of the field is also irrelevant. As shown in the proof of Lemma 4, as long as there is one control field that breaks the lattice reflection symmetry, we can always use it to decouple all mirror pairs of qubits, and thus obtain the universal gate set.

Before delving into the details of the proof, we provide some examples to enhance understanding of the theorem and explain the definition of lattice reflection symmetry breaking.

Remark 2. We can represent the one-dimensional chain as a graph $G(V, E)$ consisting of vertices V and edges E . In the graph, we place the j -th qubit on the vertex $j \in V$, and we use the edge $(j, j+1) \in E$ to represent the nearest-neighbor qubit pair having Ising-type interaction $Z_j Z_{j+1}$. Initially, all vertices and edges are uncolored. This implies that the fields applied on the vertices, i.e., H_X and H_Z , and edges, i.e., H_{ZZ} , are uniform. Then, we can use different colorings of the vertices and edges to represent the support of the additional symmetry-breaking control fields. As an example, we consider the Hamiltonians $H_{X,\alpha}$. The distinct types of lattice sites, labeled by $\alpha = A, B, C, \dots$, correspond to vertices with different colors.

Then, requiring the combined pattern formed by α to break the reflection symmetry is equivalent to demanding the graph representation to have a trivial automorphism group $\text{Aut}(G) = \{\mathbb{I}\}$, as the only nontrivial automorphism of the one-dimensional lattice graph is the reflection. As an example, if we consider $N = 8$ and $|\alpha| = 0$, i.e. no symmetry-breaking field, the graph representation is:



where we use circles and dashed lines to represent vertices and edges, respectively. The graph is invariant under reflection with respect to the axis labeled by the vertical dashed-dotted line. The reflection operator R can be represented as a product of SWAP gates:

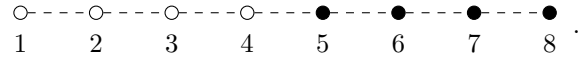
$$R = \text{SWAP}_{1,8} \text{SWAP}_{2,7} \text{SWAP}_{3,6} \text{SWAP}_{4,5}, \quad \text{where} \quad \text{SWAP}_{i,j} = \frac{1}{2} (I + X_i X_j + Y_i Y_j + Z_i Z_j), \quad (\text{B1})$$

and it is easy to verify that:

$$R Z_i R = Z_{N-i+1}, \quad R X_i R = X_{N-i+1}, \quad [R, H] = 0, \quad \text{for} \quad H \in \{H_X, H_Z, H_{ZZ}\}. \quad (\text{B2})$$

Since the system has global reflection symmetry, it cannot realize universal quantum computation.

If we apply a symmetry-breaking field $H_{X,A} = \sum_{i=5}^8 X_i$ on the right half of the chain, we can color the last four sites black, yielding the following graph representation:



The above graph has no nontrivial automorphism. According to Theorem 1, the generating set $\mathcal{G} = \{H_X, H_Z, H_{ZZ}, H_{X,A}\}$ is universal.

To prove Theorem 1, we need to show $\mathfrak{g} = \text{span}_{\mathbb{R}} \langle iH_X, iH_Z, iH_{ZZ}, \cup_i H_{X,\alpha} \rangle = \mathfrak{su}(2^N)$ if and only if the coloring represented by α breaks the lattice reflection symmetry. To reach this goal, we first present two intermediate universal sets of generators for even and odd N 's in Lemma 4. Then, in Lemma 5, we show that the generating set \mathcal{G} in Theorem 1 is equivalent to the sets in Lemma 4, which establishes our main result.

Lemma 4. Given a qubit number N , we consider the following sets of generators:

$$H_{X,j} = X_j + X_{N-j+1}, \quad H_{Z,j} = Z_j + Z_{N-j+1}, \quad H_{ZZ,j} = Z_j Z_{j+1} + Z_{N-(j+1)+1} Z_{N-j+1}, \quad \text{for } j = 1, \dots, \lfloor N/2 \rfloor. \quad (\text{B3})$$

Then, if the combined pattern formed by the subsets α on the 1D chain breaks the lattice reflection symmetry, we have a universal DLA as given by:

$$\mathfrak{su}(2^N) = \begin{cases} \text{span}_{\mathbb{R}} \langle \cup_j iH_{X,j}, \cup_j iH_{Z,j}, \cup_j iH_{ZZ,j}, \cup_{\alpha} iH_{X,\alpha} \rangle_{\text{Lie}}, & \text{for even } N \\ \text{span}_{\mathbb{R}} \langle \cup_j iH_{X,j}, \cup_j iH_{Z,j}, \cup_j iH_{ZZ,j}, \cup_{\alpha} iH_{X,\alpha}, iX_{\lfloor N/2 \rfloor + 1}, iZ_{\lfloor N/2 \rfloor + 1} \rangle_{\text{Lie}}, & \text{for odd } N \end{cases} \quad (\text{B4})$$

Remark 3. In Lemma 4, the $H_{X,j}, H_{Z,j}$ and $H_{ZZ,j}$ are reflection symmetric with respect to the center of the 1D chain. Specifically, under the reflection R , we have $RX_jR = X_{N-j+1}$ and $RZ_jR = Z_{N-j+1}$ (see Equation (B2)). Therefore, given the site j , the $H_{X,j}$ and $H_{Z,j}$ are simultaneous X - and Z -controls applied to a pair of equivalent lattice sites j and $N-j+1$. Similarly, $H_{ZZ,j}$ is the ZZ -control that is applied on two adjacent pairs of equivalent lattice sites. These Hamiltonians are also shown in Figure 1(a). When N is odd, the generators $X_{\lfloor N/2 \rfloor + 1}$ and $Z_{\lfloor N/2 \rfloor + 1}$ are only applied to the middle site of the chain, whose equivalent site is itself. We should also include them in the DLA to reach universality.

One N -qubit universal gate set is composed of single-qubit rotations generated by X_j, Z_j and two-qubit entangling gates generated by $Z_j Z_{j+1}$ for all $j \in [1, N]$ [59, 65]. According to Lemmas 2 and 3, to prove that the DLAs in Lemma 4 are universal, it suffices to show that they can generate all X_j, Z_j and $Z_j Z_{j+1}$ via commutation and linear combination. This is achievable by employing $H_{X,\alpha}$ to break the reflection symmetry, as detailed below.

Proof of Lemma 4. If the pattern formed by α breaks the lattice reflection symmetry, there must exist at least one $H_{X,\alpha'}$ that is not invariant under reflection, i.e. $RH_{X,\alpha'}R \neq H_{X,\alpha'}$. Indeed, assuming, on the contrary, $[R, H_{X,\alpha}] = 0$ for all α , the pattern formed by α preserves lattice reflection, yielding a contradiction.

For such an $H_{X,\alpha'} = \sum_{j \in \alpha'} X_j$, a uniform summation of X_j supported on α' , we claim that there must exist a $k \in \alpha'$ such that X_k and X_{N-k+1} are not simultaneously in that summation. Note that, when N is odd, this implies that $k \neq \lfloor N/2 \rfloor + 1$. Indeed, if, on the contrary, $H_{X,\alpha'}$ is a summation of terms $X_k + X_{N-k+1}$ for various k , then since $[R, X_k + X_{N-k+1}] = 0$, we must have $[R, H_{X,\alpha'}] = 0$, which contradicts the assumption that $RH_{X,\alpha'}R \neq H_{X,\alpha'}$.

Given the $H_{X,\alpha'}$, without loss of generality, we can assume $k = 1$, which implies that X_N is not in the summation in $H_{X,\alpha'}$. Therefore, we can single out Z_1 and Z_N by the following algebra:

$$Z_1 \propto [H_{X,\alpha'}, [H_{X,\alpha'}, H_{Z,1}]] = [X_1, [X_1, Z_1 + Z_N]], \quad Z_N = H_{Z,1} - Z_1.$$

Then, we can single out the individual X and ZZ terms via (using commutation relations in Equation (A3)):

$$\begin{aligned} X_1 &\propto [Z_1, [Z_1, H_{X,1}]], & X_N &\propto [Z_N, [Z_N, H_{X,1}]], \\ Z_1 Z_2 &\propto [X_1, [X_1, H_{ZZ,1}]], & Z_{N-1} Z_N &\propto [X_N, [X_N, H_{ZZ,1}]]. \end{aligned}$$

Now we have singled out all single-qubit Paulis and two-qubit ZZ gates located at both boundaries of the 1D chain. This is analogous to stripping off the leftmost and rightmost sites of the original chain. Then, we can treat the qubits located at sites $2, \dots, N-1$ as a new chain, and employ a similar strategy to single out the boundary terms again. More concretely, utilizing the ZZ interactions, we can obtain those terms as follows:

$$\begin{aligned} X_2 &\propto [Z_1 Z_2, [Z_1 Z_2, H_{X,2}]], & X_{N-1} &\propto [Z_{N-1} Z_N, [Z_{N-1} Z_N, H_{X,2}]], \\ Z_2 &\propto [X_2, [X_2, H_{Z,2}]], & Z_{N-1} &\propto [X_{N-1}, [X_{N-1}, H_{Z,2}]], \\ Z_2 Z_3 &\propto [X_2, [X_2, H_{ZZ,2}]], & Z_{N-2} Z_{N-1} &\propto [X_{N-1}, [X_{N-1}, H_{ZZ,2}]]. \end{aligned}$$

Then, repeating the above steps, we can always single out $X_{k+1}, X_{N-(k+1)+1}, Z_{k+1}, Z_{N-(k+1)+1}, Z_{k+1} Z_{k+2}$, and $Z_{N-(k+2)+1} Z_{N-(k+1)+1}$ given $Z_k Z_{k+1}, Z_{N-(k+1)+1} Z_{N-k+1}$ and the generators $H_{X,k+1}, H_{Z,k+1}, H_{ZZ,k+1}$. Therefore, all single-qubit gates and two-qubit ZZ gates are obtainable.

Before completing the proof, we have three remarks. First, the above procedure works for both even and odd N . For even N , this pairwise singling out method is always applicable, since the Pauli operators always appear in pairs, i.e. (X_k, X_{N-k+1}) and (Z_k, Z_{N-k+1}) . For odd N , we can stop when we obtain $(X_{\lfloor N/2 \rfloor}, X_{\lfloor N/2 \rfloor + 2})$ and $(Z_{\lfloor N/2 \rfloor}, Z_{\lfloor N/2 \rfloor + 2})$, because the $X_{\lfloor N/2 \rfloor + 1}$ and $Z_{\lfloor N/2 \rfloor + 1}$ are already singled out by assumption.

Second, the method is applicable to the case where $k \neq 1$. When $k = 1$, we implement the singling out procedure from the 1st level boundary to the middle ($\lfloor N/2 \rfloor$ -th level boundary) of the chain, as detailed above. When $k \neq 1$, we can start from the k -th level boundary, and perform the singling out process in both outward and inward directions. The outward and inward singling out will finally approach the 1st level boundary and the middle of the chain, respectively. During the process, all single-qubit Paulis and ZZ gates are obtained.

Third, the symmetry-breaking Hamiltonian H_{break} is not restricted to be $H_{X,\alpha}$. In our proof, we only require the H_{break} to contain a summand whose reflection pair is not simultaneously included in the summation. Then, we utilize this summand to single out the X_j or Z_j not commuting with it. Having the X_j or Z_j , we can follow the same iterative algorithm to single out all other necessary generators for a universal gate set.

Combining all above arguments, we have completed the proof. \square

From Lemma 4, if we can prove that the DLA $\mathfrak{g} = \text{span}_{\mathbb{R}} \langle iH_X, iH_Z, iH_{ZZ}, \cup_{\alpha} iH_{X,\alpha} \rangle_{\text{Lie}}$ in Theorem 1 is equal to the ones in Equation (B4), we have completed the proof of Theorem 1. Apparently, the generators $H_{X,\alpha}$ are in all DLAs, so it suffices to obtain all generators in Equation (B3). In the following lemma, we establish this key step in the proof of Theorem 1: H_X, H_Z , and H_{ZZ} generate the Hamiltonians in Equation (B3).

Lemma 5. *We have the following equivalence between DLAs:*

$$\text{span}_{\mathbb{R}}\langle iH_X, iH_Z, iH_{ZZ} \rangle_{\text{Lie}} \equiv \begin{cases} \text{span}_{\mathbb{R}}\langle \cup_j iH_{X,j}, \cup_j iH_{Z,j}, \cup_j iH_{ZZ,j} \rangle_{\text{Lie}}, & \text{for even } N \\ \text{span}_{\mathbb{R}}\langle \cup_j iH_{X,j}, \cup_j iH_{Z,j}, \cup_j iH_{ZZ,j}, \cup_i X_{\lfloor N/2 \rfloor + 1}, \cup_i Z_{\lfloor N/2 \rfloor + 1} \rangle_{\text{Lie}}, & \text{for odd } N \end{cases}, \quad (\text{B5})$$

where $H_{X,j}, H_{Z,j}$ and $H_{ZZ,j}$ are X -, Z - and ZZ - pairs given by Equation (B3), and $H_{ZZ} = \sum_{j=1}^{N-1} Z_j Z_{j+1}$, $H_Z = \sum_{j=1}^N Z_j$, $H_X = \sum_{j=1}^N X_j$.

Proof. Given H_{ZZ}, H_Z and H_X , we first obtain an H_{YY} (the uniform YY interaction) as follows:

$$\begin{aligned} H_{YZ} &= \sum_{j=1}^{N-1} Y_j Z_{j+1} + Z_j Y_{j+1} \propto [H_X, H_{ZZ}], \\ H_{YYZZ} &= \sum_{j=1}^{N-1} Y_j Y_{j+1} - Z_j Z_{j+1} \propto [H_X, H_{YZ}], \\ H_{YY} &= \sum_{j=1}^{N-1} Y_j Y_{j+1} = H_{YYZZ} + H_{ZZ}. \end{aligned} \quad (\text{B6})$$

Then, we can compute the commutator between H_{YY} and H_{ZZ} , to obtain the following intermediate Hamiltonian:

$$H_1 = \sum_{j=1}^{N-2} Z_j X_{j+1} Y_{j+2} + Y_j X_{j+1} Z_{j+2} \propto [H_{YY}, H_{ZZ}], \quad (\text{B7})$$

where we have used:

$$[Y_j Y_{j+1}, Z_j Z_{j+1}] = 0, \quad [Y_j Y_{j+1}, Z_{j+1} Z_{j+2}] = 2i Y_j X_{j+1} Z_{j+2}, \quad [Y_{j+1} Y_{j+2}, Z_j Z_{j+1}] = 2i Z_j X_{j+1} Y_{j+2}. \quad (\text{B8})$$

Then, we can compute:

$$\begin{aligned} H_2 &= H_{YY} + \sum_{j=2}^{N-2} Y_j Y_{j+1} - 2 \sum_{j=1}^{N-3} Z_j X_{j+1} X_{j+2} Z_{j+3} \propto [H_{ZZ}, H_1], \\ H_3 &= H_2 - H_{YY} = \sum_{j=2}^{N-2} Y_j Y_{j+1} - 2 \sum_{j=1}^{N-3} Z_j X_{j+1} X_{j+2} Z_{j+3}, \end{aligned} \quad (\text{B9})$$

where we have used:

$$\begin{aligned} [Z_j Z_{j+1}, Z_j X_{j+1} Y_{j+2}] &= 2i Y_{j+1} Y_{j+2}, \quad [Z_{j+1} Z_{j+2}, Y_j X_{j+1} Z_{j+2}] = 2i Y_j Y_{j+1}, \\ [Z_j Z_{j+1}, Y_{j+1} X_{j+2} Z_{j+3}] &= -2i Z_j X_{j+1} X_{j+2} Z_{j+3}, \quad [Y_{j+2} Y_{j+3}, Z_j X_{j+1} Y_{j+2}] = -2i Z_j X_{j+1} X_{j+2} Z_{j+3}. \end{aligned} \quad (\text{B10})$$

Notice that in H_3 , there are no $Y_1 Y_2$ and $Y_{N-1} Y_N$ terms, because the open boundary condition makes the boundary YY terms distinguishable from others. By doing the commutation again, we obtain:

$$\begin{aligned} H_4 &= \sum_{j=1}^{N-3} Z_j X_{j+1} Y_{j+2} + \sum_{j=2}^{N-2} Y_j X_{j+1} Z_{j+2} \propto [H_{ZZ}, H_3], \\ H_5 &= \sum_{j=2}^{N-2} Y_j Y_{j+1} - \sum_{j=1}^{N-3} Z_j X_{j+1} X_{j+2} Z_{j+3} \propto [H_{ZZ}, H_4]. \end{aligned} \quad (\text{B11})$$

Comparing H_5 to H_3 , we notice that the coefficients of the two summations are different, which implies that we can linearly combine H_3 and H_5 to single out each of the summations. Thus, we obtain:

$$\begin{aligned} \tilde{H}_{YY} &= \sum_{j=2}^{N-2} Y_j Y_{j+1} = 2H_5 - H_3, \\ H_{YY,1} &= Y_1 Y_2 + Y_{N-1} Y_N = H_{YY} - \tilde{H}_{YY}. \end{aligned} \quad (\text{B12})$$

with arbitrary coefficients which satisfy $\alpha_{ij} = \bar{\alpha}_{ji}$ and $\beta_{ij} = \bar{\beta}_{ji}$ to ensure Hermiticity.

We first investigate universal simulation in spinless fermionic systems. The following lemma provides a sufficient condition for achieving universal control over the Hilbert space \mathcal{H}_f for spinless fermions.

Lemma 7 (Example 3 of [67]). *Passive fermionic linear optics LO_f , described by $H_{\text{free},f}$, supplemented by any non-quadratic interacting Hamiltonian H_{int} containing only two-mode terms, generates the entire unitary group $U(\mathcal{H}_f)$, where $\mathcal{H}_f = \wedge^n(\mathbb{C}^d)$ is the fermionic Hilbert space with fixed particle number n and d modes.*

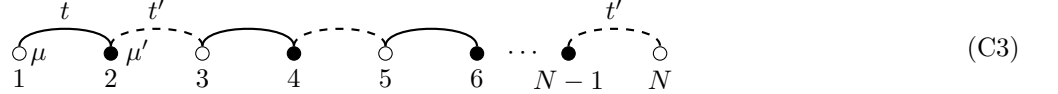
By Lemma 7, the combination of the free fermionic Hamiltonian $H_{\text{free},f}$ and a uniform nearest-neighbor Hubbard interaction

$$H_U = \sum_{i=1}^{N-1} n_i n_{i+1} \quad (\text{C2})$$

achieves universal control, where $n_i = c_i^\dagger c_i$ is the particle number operator at site i . Experimentally, fermions are typically controlled globally using optical superlattices, making the Hubbard interaction in Equation (C2) straightforward to implement. On such experimental platforms, hopping amplitudes and on-site chemical potentials are only globally addressable, resulting in periodic spatial patterns. We expect these global free Hamiltonians to generate $H_{\text{free},f}$ for universal simulation. The simplest periodic pattern, corresponding to uniform hopping amplitudes and chemical potentials, as given by

$$H^{(\text{hop})} = \sum_{i=1}^{N-1} \left(c_i^\dagger c_{i+1} + \text{h.c.} \right), \quad \text{and} \quad H^{(\mu)} = \sum_{i=1}^N n_i,$$

cannot achieve this goal since $[H^{(\text{hop})}, H^{(\mu)}] = 0$. Thus, inspired by Theorem 1, we seek the minimal periodic pattern that breaks the lattice reflection symmetry, which is the dual-site alternating pattern as illustrated in the figure below:



This alternating arrangement enables the following set of global control Hamiltonians:

$$\begin{aligned} H_{\text{odd}}^{(\text{hop})} &= \sum_{i \text{ odd}, i \neq N} \left(c_i^\dagger c_{i+1} + \text{h.c.} \right), & H_{\text{even}}^{(\text{hop})} &= \sum_{i \text{ even}} \left(c_i^\dagger c_{i+1} + \text{h.c.} \right), \\ H_{\text{odd}}^{(\mu)} &= \sum_{i \text{ odd}} n_i, & H_{\text{even}}^{(\mu)} &= \sum_{i \text{ even}} n_i, & H_U &= \sum_{i=1}^{N-1} n_i n_{i+1}, \end{aligned} \quad (\text{C4})$$

where $H_{\text{odd/even}}^{(\text{hop})}$ and $H_{\text{odd/even}}^{(\mu)}$ represent hopping amplitudes and chemical potentials on odd/even bonds and sites, respectively. As demonstrated in Theorem 8, the dual-site controls generated by the Hamiltonians in Equation (C4) enable universal simulation of spinless fermions. This again illustrates the connection between geometrical symmetry breaking and universality.

Theorem 8 (Universality of the spinless Fermi-Hubbard chain). *Consider an open-boundary spinless Fermi-Hubbard chain with an odd number N of sites. The dual-site control given by Equation (C4) achieves universal simulation of spinless fermions. Specifically, the unitary evolution generated by the dynamical Lie algebra (DLA) $\mathfrak{g} = \text{span}_{\mathbb{R}} \langle iH_{\text{odd}}^{(\text{hop})}, iH_{\text{even}}^{(\text{hop})}, iH_{\text{odd}}^{(\mu)}, iH_{\text{even}}^{(\mu)}, iH_U \rangle_{\text{Lie}}$ equals $U(\mathcal{H}_f)$, where $\mathcal{H}_f = \wedge^n(\mathbb{C}^N)$.*

Since the global interaction H_U is already included in Equation (C4), to prove Theorem 8, it suffices to demonstrate that the full passive linear optics Hamiltonian $H_{\text{free},f}$ is generated by the Hamiltonians $H_{\text{odd/even}}^{(\text{hop})}$ and $H_{\text{odd/even}}^{(\mu)}$. To accomplish this, we introduce an intermediate generating set, as stated in the following lemma:

Lemma 9. *The Hamiltonian $H_{\text{free},f}$ is generated by the following set of nearest-neighbor hopping and on-site chemical potential Hamiltonians:*

$$H_i^{(\text{hop})} = c_i^\dagger c_{i+1} + \text{h.c.}, \quad i = 1, \dots, N-1, \quad \text{and} \quad H_i^{(\mu)} = n_i = c_i^\dagger c_i, \quad i = 1, \dots, N. \quad (\text{C5})$$

Proof. The $H_{\text{free},f}$ in Equation (C1) is a linear combination of hopping and chemical potential terms, where the nearest-neighbor hoppings are given by $H_i^{(\text{hop})}$, and the on-site chemical potential terms are $H_i^{(\mu)}$, respectively. Thus, it suffices to show that the hopping term $H_{(i,j)}^{(\text{hop})} = c_i^\dagger c_j + \text{h.c.}$ between two arbitrary sites i and j can be generated by $H_i^{(\text{hop})}$ and $H_i^{(\mu)}$. The following algebra gives the hopping term between next-nearest-neighbor sites:

$$H_{(i,i+2)}^{(\text{hop})} = [H_i^{(\mu)}, [H_i^{(\text{hop})}, H_{i+1}^{(\text{hop})}]] = c_i^\dagger c_{i+2} + \text{h.c.} \quad (\text{C6})$$

Then, given the hopping between i and $i+k$ sites for an arbitrary k as $H_{i,(i,i+k)} = c_i^\dagger c_{i+k} + \text{h.c.}$, we have

$$H_{(i,i+k+1)}^{(\text{hop})} = [H_i^{(\mu)}, [H_{(i,i+k)}^{(\text{hop})}, H_{i+k}^{(\text{hop})}]] = c_i^\dagger c_{i+k+1} + \text{h.c.} \quad (\text{C7})$$

By induction, any hopping term $H_{(i,j)}^{(\text{hop})}$ can be generated by repeating the procedure, which completes the proof. \square

Now we complete the proof of Theorem 8 by generating the Hamiltonians in Equation (C5).

Proof of Theorem 8. By Lemmas 7 and 9, it suffices to prove that $H_{\text{odd/even}}^{(\text{hop})}$ and $H_{\text{odd/even}}^{(\mu)}$ can generate all hopping and chemical potential Hamiltonians $H_i^{(\text{hop})}$ and $H_i^{(\mu)}$ in (C5). This is realized by repeatedly calculating the commutator between $H_{\text{odd/even}}^{(\text{hop})}$ and $H_{\text{odd/even}}^{(\mu)}$ and hierarchically singling out the Hamiltonians $H_i^{(\text{hop})}$ and $H_i^{(\mu)}$ from both ends of the one-dimensional chain. In calculating the commutators, we repeatedly use the second relation in Equation (A3) and the fermionic canonical commutation relation (Equation (A2)).

We start by obtaining $H_1^{(\mu)} = n_1$. The following algebras are helpful:

$$\begin{aligned} [H_{\text{even}}^{(\text{hop})}, H_{\text{odd}}^{(\mu)}] &= \sum_{i \in \text{even}} [c_i^\dagger c_{i+1} + \text{h.c.}, n_{i+1}] = \sum_{i \in \text{even}} (c_i^\dagger c_{i+1} - c_{i+1}^\dagger c_i) \\ [H_{\text{odd}}^{(\mu)}, [H_{\text{even}}^{(\text{hop})}, H_{\text{odd}}^{(\mu)}]] &\propto \sum_{i \in \text{even}} (c_i^\dagger c_{i+1} + c_{i+1}^\dagger c_i) \\ H_{a,1} &= \sum_{i \in \text{even}} (n_i - n_{i+1}) \propto [[H_{\text{odd}}^{(\mu)}, [H_{\text{even}}^{(\text{hop})}, H_{\text{odd}}^{(\mu)}]], [H_{\text{even}}^{(\text{hop})}, H_{\text{odd}}^{(\mu)}]]. \end{aligned} \quad (\text{C8})$$

Notice that the ancillary Hamiltonian $H_{a,1}$ is a linear combination of number operators on different sites, except for n_1 . Thus, we can single out n_1 by:

$$H_1^{(\mu)} = H_{\text{odd}}^{(\mu)} - H_{\text{even}}^{(\mu)} + H_{a,1} = n_1. \quad (\text{C9})$$

With $H_1^{(\mu)}$, one can single out $H_1^{(\text{hop})}$ via:

$$H_1^{(\text{hop})} = c_1^\dagger c_2 + c_2^\dagger c_1 \propto [H_1^{(\mu)}, [H_{\text{odd}}^{(\text{hop})}, H_1^{(\mu)}]]. \quad (\text{C10})$$

Similarly, one can single out $H_N^{(\mu)}$ and $H_{N-1}^{(\text{hop})}$ by the following steps:

$$H_{a,N} = \sum_{i \in \text{odd}, i \neq N} (n_{i+1} - n_i) \propto [[H_{\text{odd}}^{(\mu)}, [H_{\text{odd}}^{(\text{hop})}, H_{\text{odd}}^{(\mu)}]], [H_{\text{odd}}^{(\text{hop})}, H_{\text{odd}}^{(\mu)}]] \quad (\text{C11})$$

$$H_N^{(\mu)} = H_{\text{odd}}^{(\mu)} - H_{\text{even}}^{(\mu)} + H_{a,N} = n_N, \quad H_{N-1}^{(\text{hop})} = [H_N^{(\mu)}, [H_{\text{even}}^{(\text{hop})}, H_N^{(\mu)}]] = c_{N-1}^\dagger c_N + c_N^\dagger c_{N-1}. \quad (\text{C12})$$

Then, one can define a set of new generators as:

$$\tilde{H}_{\text{odd}}^{(\text{hop})} = H_{\text{odd}}^{(\text{hop})} - H_1^{(\text{hop})} = \sum_{i \in \text{odd}, i \neq 1, N} c_i^\dagger c_{i+1} + \text{h.c.}, \quad (\text{C13})$$

$$\tilde{H}_{\text{even}}^{(\text{hop})} = H_{\text{even}}^{(\text{hop})} - H_{N-1}^{(\text{hop})} = \sum_{i \in \text{even}, i \neq N-1} c_i^\dagger c_{i+1} + \text{h.c.}, \quad (\text{C14})$$

$$\tilde{H}_{\text{odd}}^{(\mu)} = H_{\text{odd}}^{(\mu)} - H_1^{(\mu)} - H_N^{(\mu)} = \sum_{i \in \text{odd}, i \neq 1, N} n_i, \quad (\text{C15})$$

$$\tilde{H}_{\text{even}}^{(\mu)} = H_{\text{even}}^{(\mu)} = \sum_{i \in \text{even}} n_i. \quad (\text{C16})$$

These generators define a new one-dimensional chain whose two ends are the 2-nd and $(N - 1)$ -th sites in the original chain. Equivalently, this new chain can be obtained by removing the 1-st and N -th sites of the old chain. In the new chain, $\tilde{H}_{\text{odd}}^{(\text{hop})}$, $\tilde{H}_{\text{even}}^{(\text{hop})}$, $\tilde{H}_{\text{odd}}^{(\mu)}$ and $\tilde{H}_{\text{even}}^{(\mu)}$ play the same role as $H_{\text{even}}^{(\text{hop})}$, $H_{\text{odd}}^{(\text{hop})}$, $H_{\text{even}}^{(\mu)}$, $H_{\text{odd}}^{(\mu)}$ in the previous chain, i.e., the odd and even sites are exchanged. Thus, one can replace the Hamiltonians in the previous steps correspondingly to single out $H_2^{(\text{hop})}$, $H_2^{(\mu)}$, $H_{N-2}^{(\text{hop})}$, $H_{N-1}^{(\mu)}$ as:

$$H_2^{(\mu)} = n_2 \times \tilde{H}_{\text{even}}^{(\mu)} - \tilde{H}_{\text{odd}}^{(\mu)} + \frac{1}{2} [[\tilde{H}_{\text{even}}^{(\mu)}, [\tilde{H}_{\text{odd}}^{(\text{hop})}, \tilde{H}_{\text{even}}^{(\mu)}]], [\tilde{H}_{\text{odd}}^{(\text{hop})}, \tilde{H}_{\text{even}}^{(\mu)}]], \quad (\text{C17})$$

$$H_2^{(\text{hop})} = c_2^\dagger c_3 + c_3^\dagger c_2 \times [H_2^{(\mu)}, [\tilde{H}_{\text{even}}^{(\text{hop})}, H_2^{(\mu)}]], \quad (\text{C18})$$

$$H_{N-1}^{(\mu)} = n_{N-1} \times \tilde{H}_{\text{even}}^{(\mu)} - \tilde{H}_{\text{odd}}^{(\mu)} + \frac{1}{2} [[\tilde{H}_{\text{even}}^{(\mu)}, [\tilde{H}_{\text{even}}^{(\text{hop})}, \tilde{H}_{\text{even}}^{(\mu)}]], [\tilde{H}_{\text{even}}^{(\text{hop})}, \tilde{H}_{\text{even}}^{(\mu)}]], \quad (\text{C19})$$

$$H_{N-2}^{(\text{hop})} = c_{N-2}^\dagger c_{N-1} + c_{N-1} c_{N-2}^\dagger \times [H_{N-1}^{(\mu)}, [\tilde{H}_{\text{odd}}^{(\text{hop})}, H_{N-1}^{(\mu)}]]. \quad (\text{C20})$$

By repeating the above procedure to the middle of the chain, we can single out all $H_i^{(\text{hop})}$ and $H_i^{(\mu)}$ in Lemma 9. Therefore, we have completed the proof of Theorem 8. \square

The proof for the universality of spinless bosonic systems is analogous. Similar to Lemma 7, we have the following sufficient condition for achieving universal control over \mathcal{H}_b .

Lemma 10 (Adapted from Theorem 2 of [67]). *For bosonic systems with $d > 2$ modes, passive bosonic linear optics described by $H_{\text{free},b}$, supplemented by any Hamiltonian H that is not contained within the linear optics set LO_b , generates the entire unitary group $U(\mathcal{H}_b)$, where $\mathcal{H}_b = \text{Sym}^n(\mathbb{C}^d)$ is the bosonic Hilbert space with fixed particle number n .*

Since $d = N$, and for arbitrary many-body systems we always have $N > 2$, the assumption of Lemma 10 is always satisfied. In bosonic systems, the Bose-Hubbard chain with dual-site control can be readily implemented using optical superlattices, providing the following control Hamiltonians analogous to their fermionic counterparts in Equation (C4):

$$\begin{aligned} H_{\text{odd}}^{(\text{hop})} &= \sum_{i \text{ odd}, i \neq N} (b_i^\dagger b_{i+1} + \text{h.c.}), & H_{\text{even}}^{(\text{hop})} &= \sum_{i \text{ even}} (b_i^\dagger b_{i+1} + \text{h.c.}), \\ H_{\text{odd}}^{(\mu)} &= \sum_{i \text{ odd}} n_i, & H_{\text{even}}^{(\mu)} &= \sum_{i \text{ even}} n_i, & H_U &= \sum_{i=1}^{N-1} n_i (n_i - 1). \end{aligned} \quad (\text{C21})$$

As established in Theorem 11, the dual-site controls defined by Equation (C21) enable universal simulation of spinless bosons.

Theorem 11 (Universality of the spinless Bose-Hubbard chain). *Consider an open-boundary spinless Bose-Hubbard chain with an odd number of sites $N > 2$. The dual-site control provided by Equation (C21) achieves universal simulation of spinless bosons. Specifically, the DLA $\mathfrak{g} = \text{span}_{\mathbb{R}}(iH_{\text{odd}}^{(\text{hop})}, iH_{\text{even}}^{(\text{hop})}, iH_{\text{odd}}^{(\mu)}, iH_{\text{even}}^{(\mu)}, iH_U)_{\text{Lie}}$ equals $U(\mathcal{H}_b)$ generates the full unitary group $U(\mathcal{H}_b)$, where $\mathcal{H}_b = \text{Sym}^n(\mathbb{C}^N)$.*

Proof. The proof follows closely the approach used in Theorem 8. Since the Hubbard Hamiltonian H_U is not contained within the set of passive linear optics LO_b , Lemma 10 implies that it suffices to demonstrate the generation of $H_{\text{free},b}$ from the Hamiltonians $H_{\text{odd/even}}^{(\text{hop})}$ and $H_{\text{odd/even}}^{(\mu)}$. By conducting a calculation analogous to the one used in the proof of Theorem 8, but substituting the anticommutation relations of fermionic operators c^\dagger, c with the commutation relations of bosonic operators b^\dagger, b , and employing the second identity in Equation (A3), we obtain the following intermediate set of nearest-neighbor hopping and on-site chemical potential Hamiltonians:

$$H_i^{(\text{hop})} = b_i^\dagger b_{i+1} + \text{h.c.}, \quad i = 1, \dots, N-1, \quad \text{and} \quad H_i^{(\mu)} = n_i = b_i^\dagger b_i, \quad i = 1, \dots, N. \quad (\text{C22})$$

Finally, following a similar argument as in Lemma 4, one can verify that this set indeed generates $H_{\text{free},b}$, thereby completing the proof. \square

The physically relevant fermionic systems are spinful, requiring a generalization of Theorem 8 to the spinful Fermi-Hubbard chain. The generators for the one-dimensional spinful Fermi-Hubbard model on N sites (with N odd), under

open boundary conditions and dual-site superlattice control, are given by:

$$\begin{aligned}
H_{\text{odd}}^{(\text{hop})} &= \sum_{i \in \text{odd}, i \neq N, \sigma} c_{i,\sigma}^\dagger c_{i+1,\sigma} + \text{h.c.}, & H_{\text{even}}^{(\text{hop})} &= \sum_{i \in \text{even}, \sigma} c_{i,\sigma}^\dagger c_{i+1,\sigma} + \text{h.c.}, \\
H_{\text{odd}}^{(\mu)} &= \sum_{i \in \text{odd}} n_{i,\uparrow} + n_{i,\downarrow}, & H_{\text{even}}^{(\mu)} &= \sum_{i \in \text{even}} n_{i,\uparrow} + n_{i,\downarrow}, \\
H_{B_X} &= \sum_{i=1}^N c_{i,\uparrow}^\dagger c_{i,\downarrow} + \text{h.c.}, & H_{B_Z} &= \sum_{i=1}^N (a * i + b)(n_{i,\uparrow} - n_{i,\downarrow}), & H_U &= \sum_{i=1}^N n_{i,\uparrow} n_{i,\downarrow}.
\end{aligned} \tag{C23}$$

Here, $H_{\text{odd}}^{(\text{hop})}$ and $H_{\text{even}}^{(\text{hop})}$ describe spin-preserving hopping on odd and even bonds for $\sigma = \uparrow, \downarrow$. The terms $H_{\text{odd}}^{(\mu)}$ and $H_{\text{even}}^{(\mu)}$ correspond to chemical potentials on odd and even sites, respectively. H_{B_X} represents a global magnetic field along the x -axis, while H_{B_Z} corresponds to a spatially tilted magnetic field along the z -axis. Finally, H_U denotes the on-site Hubbard interaction.

As stated in Theorem 12, the dual-site controls defined by the Hamiltonians in Equation (C23) enable universal simulation of spinful fermions. A key distinction in the spinful case is that the number of modes becomes $d = 2N$, as the spin degree of freedom at each site doubles the number of modes.

Theorem 12 (Universality of the spinful Fermi-Hubbard chain). *Consider an open-boundary spinful Fermi-Hubbard chain with an odd number N of sites. The dual-site control given by Equation (C23) achieves universal simulation of spinful fermions. Specifically, the unitary evolution generated by the dynamical Lie algebra (DLA) $\mathfrak{g} = \text{span}_{\mathbb{R}} \langle iH_{\text{odd}}^{(\text{hop})}, iH_{\text{even}}^{(\text{hop})}, iH_{\text{odd}}^{(\mu)}, iH_{\text{even}}^{(\mu)}, iH_{B_X}, iH_{B_Z}, iH_U \rangle_{\text{Lie}}$ equals $U(\mathcal{H}_f)$, where $\mathcal{H}_f = \Lambda^n(\mathbb{C}^{2N})$.*

Proof. By Lemmas 7 and 9, it is sufficient to show that the set $\{iH_{\text{odd}}^{(\text{hop})}, iH_{\text{even}}^{(\text{hop})}, iH_{\text{odd}}^{(\mu)}, iH_{\text{even}}^{(\mu)}, iH_{B_X}, iH_{B_Z}\}$ can generate arbitrary free fermion gates. Without specification, we will choose $a = 1, b = 0$ for H_{B_Z} to realize the tilted z -field.

Starting with

$$[H_{\text{even}}^{(\text{hop})}, i[H_{\text{even}}^{(\text{hop})}, H_{\text{odd}}^{(\mu)}]] = \sum_{i \in \text{even}, \sigma} n_{i,\sigma} - n_{i+1,\sigma}, \tag{C24}$$

we can single out $\sum_{\sigma} n_{1,\sigma}$ by the algebra:

$$\sum_{\sigma} n_{1,\sigma} = H_{\text{odd}}^{(\mu)} - H_{\text{even}}^{(\mu)} + [H_{\text{even}}^{(\text{hop})}, [H_{\text{even}}^{(\text{hop})}, H_{\text{odd}}^{(\mu)}]]. \tag{C25}$$

By defining the following ancillary Hamiltonians:

$$\begin{aligned}
H_{a,1} &= H_{B_Z} + H_{\text{odd}}^{(\mu)} + 2H_{\text{even}}^{(\text{hop})} \\
&= 2n_{1,\uparrow} + 4n_{2,\uparrow} + \sum_{i \in \text{odd}, i \neq 1} (i+1)n_{i,\uparrow} - (i-1)n_{i,\downarrow} + \sum_{i \in \text{even}, i \neq 2} (i+2)n_{i,\uparrow} - (i-2)n_{i,\downarrow}, \\
H_{a,2} &= [H_{\text{odd}}^{(\text{hop})}, [H_{\text{odd}}^{(\text{hop})}, \sum_{\sigma} n_{1,\sigma}]] = \sum_{\sigma} (c_{1,\sigma}^\dagger c_{2,\sigma} + c_{2,\sigma}^\dagger c_{1,\sigma}),
\end{aligned} \tag{C26}$$

we can obtain $n_{2,\uparrow} - n_{1,\uparrow}$ by

$$[H_{a,2}, [H_{a,2}, H_{a,1}]] = 2(n_{2,\uparrow} - n_{1,\uparrow}). \tag{C27}$$

Then, we can use $n_{2,\uparrow} - n_{1,\uparrow}$ and the uniform B_X field to single out the B_X field on sites 1 and 2 as:

$$H_{a,3} = [n_{2,\uparrow} - n_{1,\uparrow}, [H_{B_X}, n_{2,\uparrow} - n_{1,\uparrow}]] = c_{1,\uparrow}^\dagger c_{1,\downarrow} + c_{1,\downarrow}^\dagger c_{1,\uparrow} + c_{2,\uparrow}^\dagger c_{2,\downarrow} + c_{2,\downarrow}^\dagger c_{2,\uparrow}. \tag{C28}$$

Using the uniform B_Z field by selecting $a = 0, b = 1$, i.e., $\sum_i n_{i,\uparrow} - n_{i,\downarrow}$, we construct another two ancillary Hamiltonians as:

$$\begin{aligned}
H_{a,4} &= \sum_i n_{i,\uparrow} - n_{i,\downarrow} + \sum_{\sigma} n_{1,\sigma} + \sum_{\sigma} n_{2,\sigma} = 2n_{1,\uparrow} + 2n_{2,\uparrow} + \sum_{i \neq 1,2} n_{i,\uparrow} - n_{i,\downarrow}, \\
H_{a,5} &= 2H_{a,4} - H_{a,1} = 2n_{1,\uparrow} - \sum_{i \in \text{odd}, i \neq 1} ((i+3)n_{i,\uparrow} - (i-3)n_{i,\downarrow}) - \sum_{i \in \text{even}, i \neq 2} (in_{i,\uparrow} - in_{i,\downarrow}).
\end{aligned} \tag{C29}$$

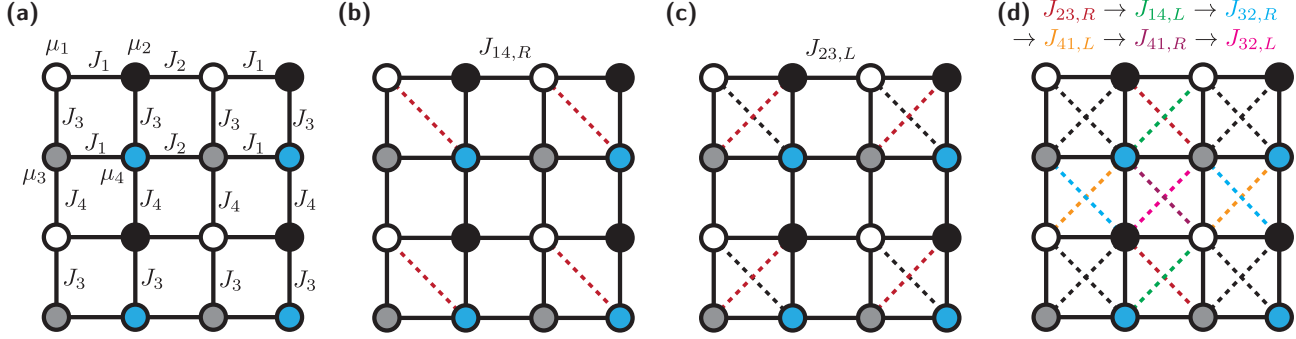


FIG. 6. Implementation of next-nearest-neighbor (NNN) hoppings in the two-dimensional Fermi-Hubbard model using global control. (a) A two-dimensional superlattice with four atomic species, labeled 1–4 and color-coded as white, black, gray, and blue, respectively. The control Hamiltonians consist of species-dependent chemical potentials $\mu_1 \sim \mu_4$ and nearest-neighbor (NN) hopping terms $J_1 \sim J_4$, indicated on the corresponding bonds. (b) Realization of the rightward NNN hopping $J_{14,R}$ between type-1 and type-4 sites, shown by red dashed lines. (c) Given $J_{14,R}$, implementation of the leftward NNN hopping $J_{23,L}$ between type-2 and type-3 sites (also in red dashed lines). (d) Sequential construction of all NNN hoppings $J_{23,R}, J_{14,L}, J_{32,R}, J_{41,L}, J_{41,R}, J_{32,L}$, indicated by colored dashed lines corresponding to the hopping types.

Then we can single out the spin flip on the first site as:

$$H_{a,6} = [H_{a,5}, [H_{a,3}, H_{a,5}]] = c_{1,\uparrow}^\dagger c_{1,\downarrow} + c_{1,\downarrow}^\dagger c_{1,\uparrow}, \quad (\text{C30})$$

which gives:

$$H_{a,7} = [[H_{a,3}, H_{a,5}], H_{a,6}] = n_{1,\uparrow} - n_{1,\downarrow}. \quad (\text{C31})$$

With $n_{1,\uparrow} + n_{1,\downarrow}$ (see Equation (C25)) and $n_{1,\uparrow} - n_{1,\downarrow}$, we can control $n_{1,\uparrow}$ and $n_{1,\downarrow}$ separately. Then, we can get the hopping between sites 1 and 2 for spin-up and spin-down individually as:

$$\begin{aligned} [[H_{\text{odd}}^{(\text{hop})}, n_{1,\uparrow}], n_{1,\uparrow}] &= c_{1,\uparrow}^\dagger c_{2,\uparrow} + c_{2,\uparrow}^\dagger c_{1,\uparrow}, \\ [[H_{\text{odd}}^{(\text{hop})}, n_{1,\downarrow}], n_{1,\downarrow}] &= c_{1,\downarrow}^\dagger c_{2,\downarrow} + c_{2,\downarrow}^\dagger c_{1,\downarrow}. \end{aligned} \quad (\text{C32})$$

Therefore, we have all individual controls on site 1 being constructed: $n_{1,\uparrow}, n_{1,\downarrow}, c_{1,\uparrow}^\dagger c_{2,\uparrow} + c_{2,\uparrow}^\dagger c_{1,\uparrow}, c_{1,\downarrow}^\dagger c_{2,\downarrow} + c_{2,\downarrow}^\dagger c_{1,\downarrow}$ and $c_{1,\uparrow}^\dagger c_{1,\downarrow} + c_{1,\downarrow}^\dagger c_{1,\uparrow}$. Following the same constructive method, one can get all individual $n_{i,\uparrow/\downarrow}$ and hopping terms. By Lemma 9, we show $\{iH_{\text{odd}}^{(\text{hop})}, iH_{\text{even}}^{(\text{hop})}, iH_{\text{odd}}^{(\mu)}, iH_{\text{even}}^{(\mu)}, iH_{B_x}, iH_{B_z}\}$ can generate all free fermion operations. Together with the onsite Hubbard interaction H_U and Lemma 7, we show that this globally controlled spinful fermionic chain is universal. \square

Appendix D: Next-Nearest-Neighbor Hoppings in the Fermi-Hubbard model

The two-dimensional Fermi-Hubbard model with next-nearest-neighbor (NNN) hoppings is widely regarded as a promising platform for capturing key features of high-temperature superconductivity. Here, we propose a protocol to implement such NNN hoppings in an analog fermionic quantum simulator based on four atomic species, as illustrated in Figure 6.

Figure 6(a) presents the superlattice geometry and the corresponding global control scheme, using a 3×3 lattice as a representative example. The superlattice consists of four distinct site types, indicated by white, black, gray, and blue nodes. Each site type i is subjected to a homogeneous, species-specific chemical potential μ_i . The nearest-neighbor hopping pattern is periodic: horizontal hoppings from odd (even) columns to the adjacent rightward even (odd) columns are controlled by J_1 (J_2), while vertical hoppings from odd (even) rows to neighboring downward even (odd) rows are governed by J_3 (J_4). This structured pattern of hopping and on-site potentials is particularly natural for implementation in fermionic optical superlattices [128].

We focus on the spinless fermion case, as the absence of a magnetic field implies that spin-up and spin-down components are dynamically decoupled. The spinful case can be straightforwardly generalized by including spin degrees of freedom. To implement the next-nearest-neighbor (NNN) hopping terms, we employ a set of global control Hamiltonians corresponding to site-dependent chemical potentials ($H_i^{(\mu)}$, $i = 1, \dots, 4$) and nearest-neighbor (NN) hopping operators ($H_i^{(\text{hop})}$, $i = 1, \dots, 4$), defined as:

$$\begin{aligned} H_1^{(\mu)} &= \sum_{i \in \text{odd}} \sum_{j \in \text{odd}} n_{i,j}, & H_2^{(\mu)} &= \sum_{i \in \text{odd}} \sum_{j \in \text{even}} n_{i,j}, & H_3^{(\mu)} &= \sum_{i \in \text{even}} \sum_{j \in \text{odd}} n_{i,j}, & H_4^{(\mu)} &= \sum_{i \in \text{even}} \sum_{j \in \text{even}} n_{i,j}, \\ H_1^{(\text{hop})} &= \sum_i \sum_{j \in \text{odd}} \left(c_{i,j+1}^\dagger c_{i,j} + \text{h.c.} \right), & H_2^{(\text{hop})} &= \sum_i \sum_{j \in \text{even}} \left(c_{i,j+1}^\dagger c_{i,j} + \text{h.c.} \right), \\ H_3^{(\text{hop})} &= \sum_{i \in \text{odd}} \sum_j \left(c_{i+1,j}^\dagger c_{i,j} + \text{h.c.} \right), & H_4^{(\text{hop})} &= \sum_{i \in \text{even}} \sum_j \left(c_{i+1,j}^\dagger c_{i,j} + \text{h.c.} \right). \end{aligned} \quad (\text{D1})$$

To engineer the rightward NNN hopping between type-1 and type-4 sites, as shown in Figure 6(b), we begin by isolating the appropriate NN hopping terms using commutators with the chemical potential Hamiltonians:

$$H_1^{(\text{hop})'} = i[H_2^{(\mu)}, H_1^{(\text{hop})}] = i \sum_{i \in \text{odd}} \sum_{j \in \text{odd}} \left(c_{i,j+1}^\dagger c_{i,j} - c_{i,j}^\dagger c_{i,j+1} \right), \quad (\text{D2})$$

$$H_3^{(\text{hop})'} = i[H_4^{(\mu)}, H_3^{(\text{hop})}] = i \sum_{i \in \text{odd}} \sum_{j \in \text{even}} \left(c_{i+1,j}^\dagger c_{i,j} - c_{i,j}^\dagger c_{i+1,j} \right). \quad (\text{D3})$$

Their nested commutator yields an imaginary NNN hopping:

$$H_{14,R}^{(\text{hop})'} = i[H_1^{(\text{hop})'}, H_3^{(\text{hop})'}] = i \sum_{i \in \text{odd}} \sum_{j \in \text{odd}} \left(c_{i+1,j+1}^\dagger c_{i,j} - c_{i,j}^\dagger c_{i+1,j+1} \right). \quad (\text{D4})$$

To obtain a Hermitian NNN hopping, we eliminate the imaginary prefactor using a final commutator with a chemical potential term:

$$H_{14,R}^{(\text{NNN})} = i[H_1^{(\mu)}, H_{14,R}^{(\text{hop})'}] = \sum_{i \in \text{odd}} \sum_{j \in \text{odd}} \left(c_{i+1,j+1}^\dagger c_{i,j} + c_{i,j}^\dagger c_{i+1,j+1} \right). \quad (\text{D5})$$

Thus, the rightward NNN hopping term $H_{14,R}^{(\text{NNN})}$ is obtained via the triple nested commutator:

$$H_{14,R}^{(\text{NNN})} = [H_1^{(\mu)}, [[H_2^{(\mu)}, H_1^{(\text{hop})}], [H_4^{(\mu)}, H_3^{(\text{hop})}]]]. \quad (\text{D6})$$

Similarly, the leftward NNN hopping between type-2 and type-3 sites, depicted in Figure 6(c), is given by:

$$H_{23,L}^{(\text{NNN})} = [H_2^{(\mu)}, [[H_1^{(\mu)}, H_1^{(\text{hop})}], [H_3^{(\mu)}, H_3^{(\text{hop})}]]]. \quad (\text{D7})$$

Together, these two terms realize the NNN hoppings on a single plaquette, and the remaining six NNN hoppings can be obtained analogously using the following expressions:

$$H_{23,R}^{(\text{NNN})} = [H_2^{(\mu)}, [[H_1^{(\mu)}, H_2^{(\text{hop})}], [H_3^{(\mu)}, H_3^{(\text{hop})}]]], \quad (\text{D8})$$

$$H_{14,L}^{(\text{NNN})} = [H_1^{(\mu)}, [[H_2^{(\mu)}, H_2^{(\text{hop})}], [H_4^{(\mu)}, H_3^{(\text{hop})}]]], \quad (\text{D9})$$

$$H_{32,R}^{(\text{NNN})} = [H_3^{(\mu)}, [[H_4^{(\mu)}, H_1^{(\text{hop})}], [H_2^{(\mu)}, H_4^{(\text{hop})}]]], \quad (\text{D10})$$

$$H_{41,L}^{(\text{NNN})} = [H_4^{(\mu)}, [[H_3^{(\mu)}, H_1^{(\text{hop})}], [H_1^{(\mu)}, H_4^{(\text{hop})}]]], \quad (\text{D11})$$

$$H_{41,R}^{(\text{NNN})} = [H_4^{(\mu)}, [[H_3^{(\mu)}, H_2^{(\text{hop})}], [H_1^{(\mu)}, H_4^{(\text{hop})}]]], \quad (\text{D12})$$

$$H_{32,L}^{(\text{NNN})} = [H_3^{(\mu)}, [[H_4^{(\mu)}, H_2^{(\text{hop})}], [H_2^{(\mu)}, H_4^{(\text{hop})}]]]. \quad (\text{D13})$$

These expressions follow a clear structural rule: for a given NNN hopping $H_{ij,L/R}^{(\text{NNN})}$, we identify a two-step path from site i to j via an intermediate site k , such that the three chemical potential Hamiltonians correspond to $H_i^{(\mu)}, H_k^{(\mu)}, H_j^{(\mu)}$, and the NN hopping operators correspond to the two bonds along the path. The order of commutators reflects this path structure.

With all NNN hopping terms constructed, we can implement the full NNN Fermi-Hubbard Hamiltonian using Trotterized evolution, as described in Lemmas 2 and 3. This approach enables the efficient analogue simulation of strongly correlated electron systems, including candidate models for high-temperature superconductivity.

Appendix E: Symmetry-Protected-Topological Phases

The effective Hamiltonian we focus on is the cluster-Ising model:

$$H_{ZXZ} = J_{\text{eff}} \sum_i Z_{i-1} X_i Z_{i+1}, \quad (\text{E1})$$

which serves as a pedagogical example of a system realizing a symmetry-protected topological (SPT) phase. Through the Jordan-Wigner transformation, this model can be mapped to a pair of decoupled Kitaev chains [51, 89], supporting a topological edge mode, as illustrated in Figure 2(a). When the total number of sites N is even, the Hamiltonian in Equation (E1) respects a $\mathbb{Z}_2 \times \mathbb{Z}_2$ symmetry generated by the operators $P_1 = X_1 X_3 X_5 \cdots X_{N-1}$ and $P_2 = X_2 X_4 X_6 \cdots X_N$. Although P_1 and P_2 are non-local, their action in the ground-state subspace is effectively localized near the boundaries. Specifically, they reduce to boundary operators: $P_1^{(L)} = X_1 Z_2$, $P_1^{(R)} = Z_N$ and $P_2^{(L)} = Z_1$, $P_2^{(R)} = Z_{N-1} X_N$. Notably, the boundary operators $P_1^{(L)}$ and $P_2^{(L)}$ are anti-commuting symmetries on the boundary, which confirms the presence of degenerate topological edge modes in the cluster-Ising model. In the following, we show that using quantum optimal control, it is possible to design a sequence of global control pulses $u_\alpha^{(\tau)}(t)$ such that

$$\mathcal{T} \left[e^{-i \int dt \sum_\alpha u_\alpha^{(\tau)}(t) H_\alpha} \right] = e^{-i\tau H_{ZXZ}} \quad (\text{E2})$$

realizing the target unitary evolution under the cluster-Ising

1. The limitation of quantum simulation in the blockade regime

Most current quantum simulation experiments using Rydberg atoms operate in the blockade regime, where the V_{jl} in Equation (10) is sufficiently large for adjacent sites j and l , so the neighboring atoms cannot be excited simultaneously. In this regime, the system is effectively governed by the PXP model Hamiltonian [53, 129]:

$$H_{PXP} = \frac{\Omega(t)}{2} \sum_{i=2}^{N-1} P_{i-1} X_i P_{i+1} - \Delta(t) \sum_{i=1}^N n_i, \quad (\text{E3})$$

where $\Omega(t)$ and $\Delta(t)$ are the global Rabi frequency and detuning as in Equation (10), respectively. In Equation (E3), $P_i = \frac{1}{2}(I_i + Z_i)$ is the projector to the $|0\rangle$ subspace at the site i , and $n_i = I_i - P_i = \frac{1}{2}(I_i - Z_i)$ is the number operator.

Here, we prove that the PXP model cannot generate the dynamics of the ZXZ model described by Equation (E1). If we define the control Hamiltonians of H_{PXP} as

$$H_\Omega = \sum_{i=2}^{N-1} P_{i-1} X_i P_{i+1}, \quad H_\Delta = \sum_{i=1}^N n_i, \quad (\text{E4})$$

we will prove the following proposition:

Proposition 1. *Consider a chain of qubits. Given the quantum control described by the PXP model in Equation (E3), one cannot simulate the dynamics of the ZXZ Hamiltonian in Equation (E1).*

Proof. It suffices to show that there is one evolution by H_{ZXZ} that is not attainable by H_{PXP} . For the chain with N qubits, we define the computational basis states as $\{|s\rangle\}$ for all binary strings $\mathbf{s} \in \mathbb{F}_2^N$. We define a doubly-excited state as the computational basis states $|s\rangle$ with at least two consecutive 1's in the string \mathbf{s} , such as $|1100 \dots 00\rangle$ and $|11100 \dots 0\rangle$.

If the qubit chain is initialized to the all 0 state $|0\rangle^{\otimes N}$, using the PXP control Hamiltonians in Equation (E4), we cannot evolve the system to any doubly-excited state, a defining property of the PXP model, as illustrated initially in [129]. To see this, we first notice that H_Δ is diagonal in the computational basis, so we focus on the evolution generated by H_Ω . For the i -th qubit, there is only one term, $P_{i-1} X_i P_{i+1}$, that flips it along the X -axis. The flipping happens when the neighboring qubits at sites $i-1$ and $i+1$ are both at the $|0\rangle$ state, a constraint imposed by the projectors P_{i-1} and P_{i+1} . This prohibits the evolution from $|0\rangle^{\otimes N}$ to any doubly-excited state.

However, one can use H_{ZXZ} to evolve $|0\rangle^{\otimes N}$ to a doubly excited state $|\phi\rangle \equiv |011 \dots 10\rangle$ where there are $(N-2)$ consecutive $|1\rangle$'s between the two $|0\rangle$'s at both ends. To see this, we notice that:

$$H_{ZXZ} = \sum_{i=2}^{N-1} Z_{i-1} X_i Z_{i+1} = U_{CZ} \left(\sum_{i=2}^{N-1} X_i \right) U_{CZ}, \quad \text{with} \quad U_{CZ} = \prod_{i=1}^{N-1} CZ_{i,i+1}, \quad (\text{E5})$$

where $CZ_{i,i+1}$ is the controlled-Z gate between the i -th and $(i+1)$ -th qubits, which has the following algebra with Pauli operators:

$$CZ_{i,i+1} \cdot X_i \cdot CZ_{i,i+1} = X_i Z_{i+1}, \quad CZ_{i,i+1} \cdot X_{i+1} \cdot CZ_{i,i+1} = Z_i X_{i+1}. \quad (\text{E6})$$

Utilizing the fact that $U_{CZ} |0\rangle^{\otimes N} = 0$ and $U_{CZ} |\phi\rangle = (-1)^{N-3} |\phi\rangle$, we find that a $\frac{\pi}{2}$ -evolution by H_{ZXX} can evolve $|0\rangle^{\otimes N}$ to $|\phi\rangle$ as (using $U_{CZ}^2 = I$)

$$\begin{aligned} \langle \phi | e^{-i\frac{\pi}{2} H_{ZXX}} |0\rangle^{\otimes N} &= \langle \phi | U_{CZ} e^{-i\frac{\pi}{2} \sum_{i=2}^{N-1} X_i} U_{CZ} |0\rangle^{\otimes N} = (-1)^{N-3} \langle \phi | \prod_{i=2}^{N-1} e^{-i\frac{\pi}{2} X_i} |0\rangle^{\otimes N} \\ &= (-1)^{N-3} \langle \phi | \prod_{i=2}^{N-1} (-i) X_i |0\rangle^{\otimes N} = (-1)^{N-3} (-i)^{N-2}. \end{aligned} \quad (\text{E7})$$

Up to a physically irrelevant phase factor $(-1)^{N-3} (-i)^{N-2}$, we evolve $|0\rangle^{\otimes N}$ to $|\phi\rangle$, a task impossible for the PXP model. Therefore, we reach our conclusion. \square

Appendix F: Direct Trajectory Optimization

Quantum optimal control describes an optimization problem over the space of time-dependent state and control *trajectories* subject to the Schrödinger equation. The goal of a quantum optimal control problem is to return controls $u(t)$ such that the generator of the dynamics—the Hamiltonian $H[\mathbf{u}(t)]$ —drives the quantum state to a desired form: for a state vector, that form might be a specific state preparation, while for a unitary propagator, it might be a high-fidelity gate. In all but the simplest scenarios, $H[\mathbf{u}(t)]$ induces dynamics involving many non-commuting Hamiltonian terms. Analytic controls $u(t)$ are not easily found, and numerical approaches are necessary.

Trajectory optimization problems are an umbrella term for this category of optimization problem. The core structure is

$$\min_{x(t), u(t)} \int_0^T dt \ell(x(t), u(t)) + \ell_T(x(T)) \quad (\text{F1})$$

$$\text{s.t.} \quad \dot{x} = f(x(t), u(t), t) \quad (\text{F2})$$

$$x(0) = x_{\text{init}} \quad (\text{F3})$$

Here, $x(t)$ is the state trajectory, $u(t)$ is the control trajectory, $t \in [0, T]$, $\ell(\cdot, \cdot)$ is an arbitrary objective function along the entire trajectory, and $\ell_T(\cdot)$ is a terminal objective. A typical terminal objective measures the distance between $x(T)$ and a goal state, x_{goal} . In practice, trajectory optimization problems can be solved numerically by first discretizing time into N intervals, with the trajectory data retained as N *knot points* $z_k = (x_k, u_k)$, $k \in \{1 \dots N\}$. The dynamics, Eq. (F2), are enforced between knot points over each interval $[t_k, t_k + \Delta t_k]$, such that $x_{k+1} = F(x_k, u_k, t_k, \Delta t_k) = x_k + \int_{t_k}^{t_k + \Delta t_k} dt f(x(t), u(t), t)$.

A common approach in quantum optimal control is to solve F1 using *indirect* trajectory optimization, i.e., optimizing solely over the control variables $u_{1:N-1}$:

$$\text{minimize}_{u_{1:N-1}} \sum_{k=1}^{N-1} \ell(x_k(u_{1:k-1}), u_k) + \ell_T(x_N(u_{1:N-1})) \quad (\text{F4})$$

$$\text{subject to} \quad |u(t)| \leq u_{\text{max}} \quad (\text{F5})$$

where it is natural to add bound constraints on the controls, Eq. (F5). The GRAPE algorithm [130] is the most well-known example. Advantageously, indirect approaches involve a relatively small number of optimization variables because controls are fewer in dimension than states. However, the cost of this advantage is paid in function evaluations, as each x_k must be retrieved by evolving the initial state according to the dynamics. This evolution becomes a part of any gradients involving x_k , which must propagate its dependence on $u_{1:k-1}$, making constraints on intermediate states difficult to enforce. Moreover, the cost landscape over the space of control trajectories becomes highly nonlinear and challenging to navigate [131, 132].

In robotics and aerospace engineering, offline control problems like Eq. (F1) are often solved using *direct* trajectory optimization methods. The direct approach treats the state variables $x_{1:N}$ as optimization variables alongside the

controls $u_{1:N-1}$, e.g., Ref. [43, 44]:

$$\underset{x_{1:N}, u_{1:N-1}}{\text{minimize}} \quad \sum_{k=1}^{N-1} \ell(x_k, u_k) + \ell_T(x_N) \quad (\text{F6})$$

$$\text{subject to} \quad x_{k+1} = F(x_k, u_k, t_k, \Delta t_k) \quad (\text{F7})$$

$$c(x_k, u_k) \leq 0 \quad (\text{F8})$$

$$x_1 = x_{\text{init}} \quad (\text{F9})$$

where F in Eq. (F7) denotes the dynamics, which is enforced as a nonlinear constraint. We include this dynamics constraint alongside arbitrary non-linear constraints, represented by Eq. (F8) and encompassing the bounds constraints on controls. Both constraints are handled by solving Eq. (F6) using a modern nonlinear optimization tool like IPOPT [133], which is expressly designed for large-scale nonlinear programming with constraints. Direct methods have a significant structural advantage over indirect methods when functions of the state variables are required because the gradients will depend directly on x_k . Indeed, direct methods offer much finer control over properties like smoothness, time-optimality, and robustness that inform the design of the final controls [134, 135]. Moreover, the cost landscape of $z_{1:N}$ is fundamentally different from the landscape over $u_{1:N}$, critical for navigating highly constrained spaces [44]. For the case of unitary optimal control, we set up the following direct trajectory optimization problem:

$$\underset{z_{1:N}}{\text{minimize}} \quad \sum_k J(z_k) + Q\left(1 - \mathcal{F}\left(\vec{U}_N\right)\right) \quad (\text{F10})$$

$$\text{subject to} \quad \vec{U}_{k+1} = \Phi\left(\vec{U}_k, u_k, \dot{u}_k, t_k, \Delta t_k\right) \quad (\text{F11})$$

$$u_{k+1} = u_k + \dot{u}_k \Delta t_k \quad (\text{F12})$$

$$\dot{u}_{k+1} = \dot{u}_k + \ddot{u}_k \Delta t_k \quad (\text{F13})$$

$$|\ddot{u}_k| < \ddot{u}_{\text{max}} \quad (\text{F14})$$

$$t_{k+1} = t_k + \Delta t_k \quad (\text{F15})$$

$$\vec{U}_1 = \text{isovec}(I) \quad (\text{F16})$$

where

$$z_k = \begin{pmatrix} \vec{U}_k \\ u_k \\ \dot{u}_k \\ \ddot{u}_k \\ t_k \\ \Delta t_k \end{pmatrix} \quad \text{and} \quad \vec{U}_k = \text{isovec}(U_k) = \text{vec} \begin{pmatrix} \text{Re}(U_k) \\ \text{Im}(U_k) \end{pmatrix} \quad (\text{F17})$$

To set up and solve Eq. (F10), we use `Piccolo.jl` [136], a state-of-the-art software ecosystem addressing quantum optimal control using direct trajectory optimization.

Control pulses that vary smoothly over a parameterized gate family can be obtained by solving a coordinated quantum optimal control problem and interpolating the results [134, 137, 138]. If the interpolated representation is a neural network, efficient calibration of the entire control manifold implementing the gate family is possible [134].

Appendix G: Quantum Optimal Control Performance

To evaluate the performance of direct quantum optimal control, we also prepared pulses using Gradient Ascent Pulse Engineering (GRAPE), an *indirect* quantum optimal control method. We outline our implementation of GRAPE in this section.

Our pulse parameters consist of the intermediate values of $\Omega(t)$ and $\Delta(t)$ (as the values at $t = 0$ and $t = T$ are fixed to be zero). Between these intermediate points, the controls are linearly interpolated to produce piecewise linear pulses. To respect the time resolution available on Aquila, in total there are 48 parameters for a pulse of length $T = 1.25\mu\text{s}$, with 24 parameters each for the detuning and Rabi frequency. We fix the interatomic spacing to be $8.9\mu\text{m}$, the same value used for the direct method of pulse optimization. We utilized the Adam optimizer available in JAX to minimize the following loss function:

$$\ell = 1 - \langle F_i \rangle_i + \lambda \sum_k g_k + r \sum_\alpha \left\langle \frac{d^2 u_\alpha}{dt^2} \right\rangle_t \quad (\text{G1})$$

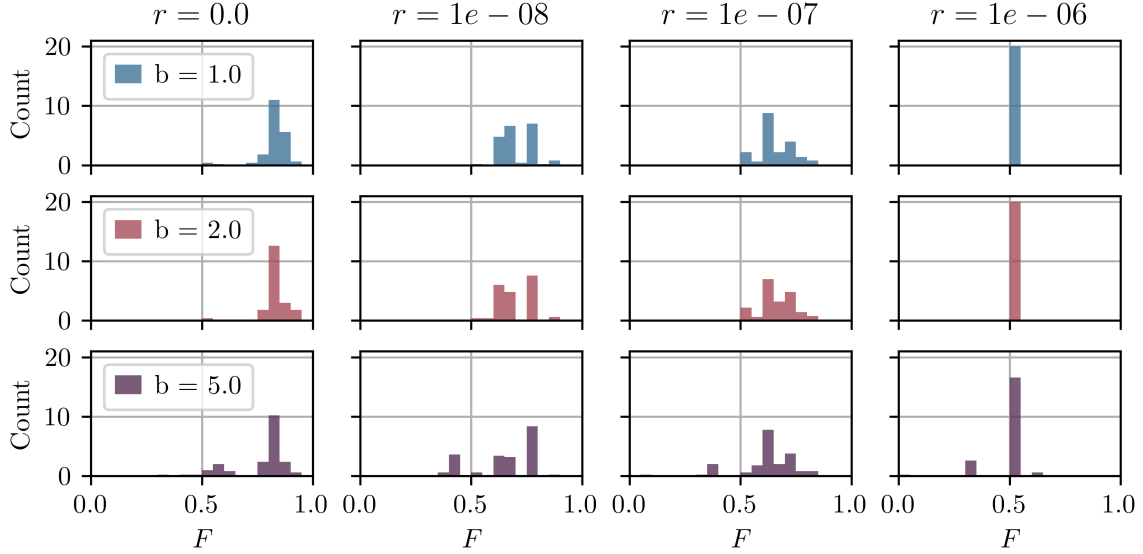


FIG. 7. **GRAPE simulation data.** The second derivative regularization (r) is varied across columns and the spread of the random initialization (b) is varied across rows. No appreciable dependence on b is found in simulation, but the value of r can highly influence the optimized pulse. Smaller values of r tend to produce higher fidelity pulses; however, these solutions are increasingly non-smooth.

Here, F_i refers to the fidelity between a Haar random state $|\phi_i\rangle$ evolved under the target H_{ZXZ} Hamiltonian for $\tau = 0.8$ and the same Haar random state evolved under the the global control pulse for the native Hamiltonian. We average over fifty states $|\phi_i\rangle$ in total. Physical constraints on the value and first derivative of the control are encoded via the quadratic penalty functions g_k , which remain zero unless the upper or lower bounds are violated. If any violations occur, the difference between violated bound and the value is squared and added to g_k , which is then weighted by $\lambda = 100$ to encourage respecting the physical constraints. Finally, r is a regularization weighting the average second derivative of the control to encourage smoothness in the controls u_α . We vary r between 0.0 and 1e-6.

We perform 100 optimization trials with the initial values for u_α randomly selected from a uniform distribution, using bounds $(0, b)$ for $\Omega(t)$ and $(-b, b)$ for $\Delta(t)$. After generating 100 optimization trials each for $b = 1, 2,$ and 5 , we determined that there is little dependence on optimization range. These results are provided in Fig. 7 The optimized pulses are more heavily dependent on the regularization r ; this dependence is visualized in Fig. 3 of the main text.

Appendix H: Additional experimental results

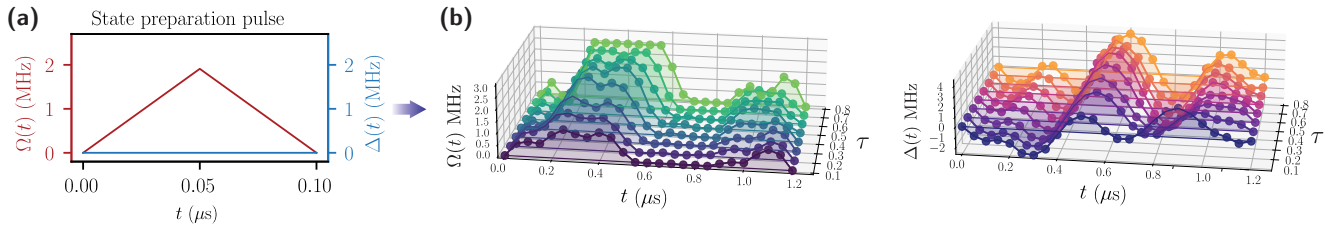


FIG. 8. **Control pulses for additional experiments.** (a) State preparation pulse used to initialize the Λ -state, a different initial state for benchmarking. (b) Replotted control pulses from Figure 2(c) used to engineer the ZXZ Hamiltonian dynamics, shown as a function of effective time τ .

In this subsection, we provide additional experimental details. The Rydberg atom array platform used in our experiments is provided by QuEra Computing. Further information can be found in the Aquila white paper [90]. Table I summarizes the key control parameters and constraints relevant to our work. Note that in the white paper, the unit for the Rabi frequency is given in $\text{rad}/\mu\text{s}$, with the conversion $2\pi (\text{rad}/\mu\text{s}) = 1 \text{ MHz}$.

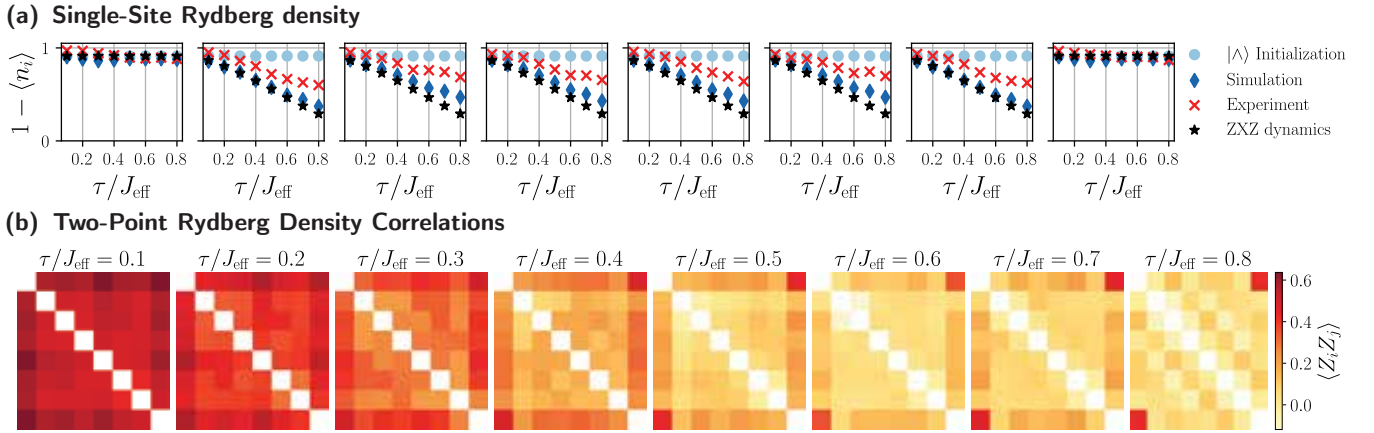


FIG. 9. **Additional experimental signatures of topological dynamics.** (a) Single-site Rydberg densities after applying the optimized global pulse [Figure 2(c), Figure 8(b)] to an 8-atom chain initialized in the Λ -state using the state preparation pulse in Figure 8(a). Boundary atoms (1 and 8) retain high populations, while bulk atoms exhibit decay with increasing τ/J_{eff} , consistent with edge mode dynamics of the ZXZ Hamiltonian (black stars). Experimental data (red crosses) agrees with ideal simulations (blue diamonds). (b) Connected two-point correlations $\langle Z_i Z_j \rangle$ measured at various τ/J_{eff} , showing persistent edge-edge correlations in experiment, in agreement with theoretical predictions. The size of the experimental error bars (standard deviation) is smaller than that of the red cross markers.

Due to hardware limitations discussed in the main text, we are restricted to measurements in the Pauli- Z basis by detecting the Rydberg density of each atom. This constraint prevents access to information in other bases, limiting our ability to directly probe other topological edge signatures. To address this, we applied our control protocol to different initial states by prepending an additional short-duration global control pulse prior to the effective ZXZ dynamics. Specifically, we used the global pulse shown in Figure 8(a) to prepare a distinct initial state, which we refer to as the Λ -state due to the shape of the pulse.

Prepending a state preparation pulse increases the total duration of the experiment and can introduce additional decoherence. To minimize this effect, we designed the pulse in Figure 8(a) to ramp the Rabi frequency up to near its maximum and then quickly back down. The corresponding experimental results are shown in Figure 9. In subplot (a), we observe good agreement between experiment and ideal simulation for the edge atoms, which maintain high Rydberg density, while the bulk atoms show slight deviations, possibly due to control errors. In subplot (b), persistent edge-edge correlations between the two boundary atoms are also observed, consistent with the expected topological behavior.

| Description | Constraint |
|----------------------------------|---|
| Rabi frequency bounds | $0 < \Omega < 2.41$ MHz |
| Detuning range | $-19.9 < \Delta < 19.9$ MHz |
| Maximum Rabi frequency slew rate | $ \delta\Omega/\delta t < 39.7$ MHz/ μ s |
| Maximum detuning slew rate | $ \delta\Delta/\delta t < 397$ MHz/ μ s |
| Minimum time resolution | $\delta t \geq 0.05$ μ s |

TABLE I. System control constraints for laser pulse shaping.